Journal of Porphyrins and Phthalocyanines
J. Porphyrins Phthalocyanines 2018; **22**: 1–23
DOI: 10.1142/S108842461850092X

Published at http://www.worldscinet.com/jpp/

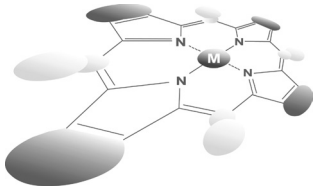

Discotic liquid crystals of transition metal complexes 56†: Synthesis of mesogenic phthalocyanine-fullerene dyads and influence of the substitution position of alkoxy chains and the kind of terminal groups on appearance of the helical supramolecular structure

Kohei Ishikawa[a], Ayumi Watarai[a], Mikio Yasutake[b] and Kazuchika Ohta*[a]

[a]*Smart Material Science and Technology, Interdisciplinary Graduate School of Science and Technology, Shinshu University, 1-15-1 Tokida, Ueda, 386-8567, Japan*
[b]*Comprehensive Analysis Center for Science, Saitama University, 255 Shimo-okubo, Sakura-ku, Saitama 338-8570, Japan*

Received 23 May 2018
Accepted 21 June 2018

ABSTRACT: We have synthesized twelve novel discotic columnar liquid crystals based on a phenoxy-group-substituted phthalocyaninato copper(II) complex having the same alkoxy chain of $C_{16}H_{33}O$ at different positions in the phenoxy group: the parent compounds {**0a~0c-16**} and the OH-substituted compounds {**3a~3c-16**}, the OFBA-substituted compounds {**2a~2c-16**} and the C_{60}-substituted dyads {**1a~1c-16**}. The letters of **a**, **b** and **c** mean substitution positions of $C_{16}H_{33}O$ group at *m*-, *p*- and *m,p*-, respectively. We have investigated the influence of both substitution position of the alkoxy chains and the kind of terminal groups (OH, OFBA and C_{60}) on the mesomorphism and the helical supramolecular structure, by using DSC, POM and temperature-variable small angle X-ray diffraction measurements. As a result, an additional big peak (Peak H) tends to appear at around $2\theta = 1.1°$ in the X-ray diffraction patterns only for the dyads {**1a~1c-16**} but not for the other compounds, {**0a~0c-16**}, {**3a~3c-16**} and {**2a~2c-16**}, regardless of the substitution positions of the alkoxy group. Moreover, we revealed that both the *m-substituted* derivative **1a-16** and the *m,p-substituted* derivative **1c-16** gave Peak H, but that only the *p-substituted* derivative **1b-16** did not give Peak H among these three dyads {**1a~1c-16**}. From the temperature-variable small angle X-ray diffraction measurements for the *m,p-substituted* derivative **1c-16** using two different sample preparation methods, we proved that the Peak H originates from a helical pitch of fullerenes. We also pointed out that the *m-substituted* long alkoxy chains are at least needed to form the helical supramolecular structure in the present $(PhO)_6PcM$-C_{60}-based dyads.

KEYWORDS: phthalocyanine, fullerene, columnar mesophase, homeotropic alignment, helical supramolecular structure, substitution position effect.

INTRODUCTION

In recent years, liquid crystalline dyads covalently bonded between a donor (D) molecule and an acceptor (A) molecule have been investigated toward high conversion efficiency of organic thin film solar cells [2–26]. Such a D–A liquid crystalline dyad may provide efficient charge separation within a molecule. If the D–A liquid crystalline dyad would additionally show spontaneous perfect homeotropic alignment between two electrode plates, one dimensional nano-array structure [27] would be achieved to realize much higher conversion efficiency. However,

*Correspondence to: Kazuchika Ohta, tel.: +81 268-24-2796, fax: +81 268-24-2796, email: ko52517@shinshu-u.ac.jp.

†Part 54: Ref. [1].

the relationship between the molecular structures of dyads and the liquid crystalline phase supramolecular structures has never been clarified to date.

In 2007, we succeeded for the first time the synthesis of phthalocyanine-fullerene (Pc-C_{60}) dyads showing perfect homeotropic alignment [3]. Thereafter, we have synthesized several kinds of liquid crystalline Pc-C_{60} dyads, and found that some of them also showed a perfect homeotropic alignment [5, 8, 9, 11–14, 19–22, 24, 25]. During our research on such liquid crystalline Pc-C_{60} dyads, we accidentally found that the spherical C_{60} moieties helically pile up around the column formed by disk-like Pc moieties in some of these columnar mesophases. The helical supramolecular structure was established by using temperature-variable small angle X-ray diffraction measurements [5, 8, 9, 11–14, 21, 22, 24, 25]. Figure 1[a] illustrates a series of the liquid crystalline Pc-C_{60} dyads [*m,p*-$(C_{12}O)_2PhO]_6$PcM-C_m-C_{60} (M = Co, Ni, Cu; *m* = 6,8,10,12), which show helical stack of the C_{60} moieties around the column formed by the Pc moieties (see Fig. 1). The small angle X-ray diffraction gave an additional big peak due to the helical pitch (hereafter named as Peak H) in the extremely low angle region around $2\theta \cong 1.0°$ (= *ca.* 80 Å) [21]. Furthermore, we synthesized another novel series of liquid crystalline Pc-C_{60} dyads $(C_nS)_6$PcCu-C_m-C_{60} illustrated in Fig. 1[b], and they also formed a helical supramolecular structure for C_{60} moieties and gave a big Peak H in the X-ray diffraction patterns [22, 24]. By using both Method A (for random alignment) and Method C (for homeotropic alignment) for the same sample, it was proven that the Peak H originates from a helical pitch of C_{60} moieties [21, 22, 24, 25]. The helical supramolecular structure model is illustrated in the lower left of Fig. 1. This unique structure resembles a spiranthes flower shown in the lower right of Fig. 1, so that it was named "spiranthes-like supramolecular structure" [22, 24, 25].

In 2010, another research group synthesized a *p-substituted* $(PhO)_6$PcM-C_{60}-based dyad (*p*-$C_{12}OPhO)_6$-PcZn-OPh-C_{60} [= ZnPc-C_{60}], which very much resembled our *m,p-substituted* dyads [*m,p*-$(C_{12}O)_2PhO]_6$PcM-C_m-C_{60}, and they also reported that spherical C_{60} moieties were helically stacked around the column formed by disk-like Pc moieties [10, 15, 16, 26]. This *p-substituted* dyad showed a Peak H as only a very small shoulder (see Fig. 2(d) in Ref. 16), whereas our *m,p-substituted* dyads showed it as an extremely big clear peak [21, 22, 24, 25]. Moreover, this PcZn-C_{60} dyad shows only rectangular columnar (Col_r) phases, so that the dyad cannot achieve homeotropic alignment. In principle, only hexagonal columnar (Col_h) and tetragonal columnar (Col_{tet}) phases can give a homeotropically aligned samples [28].

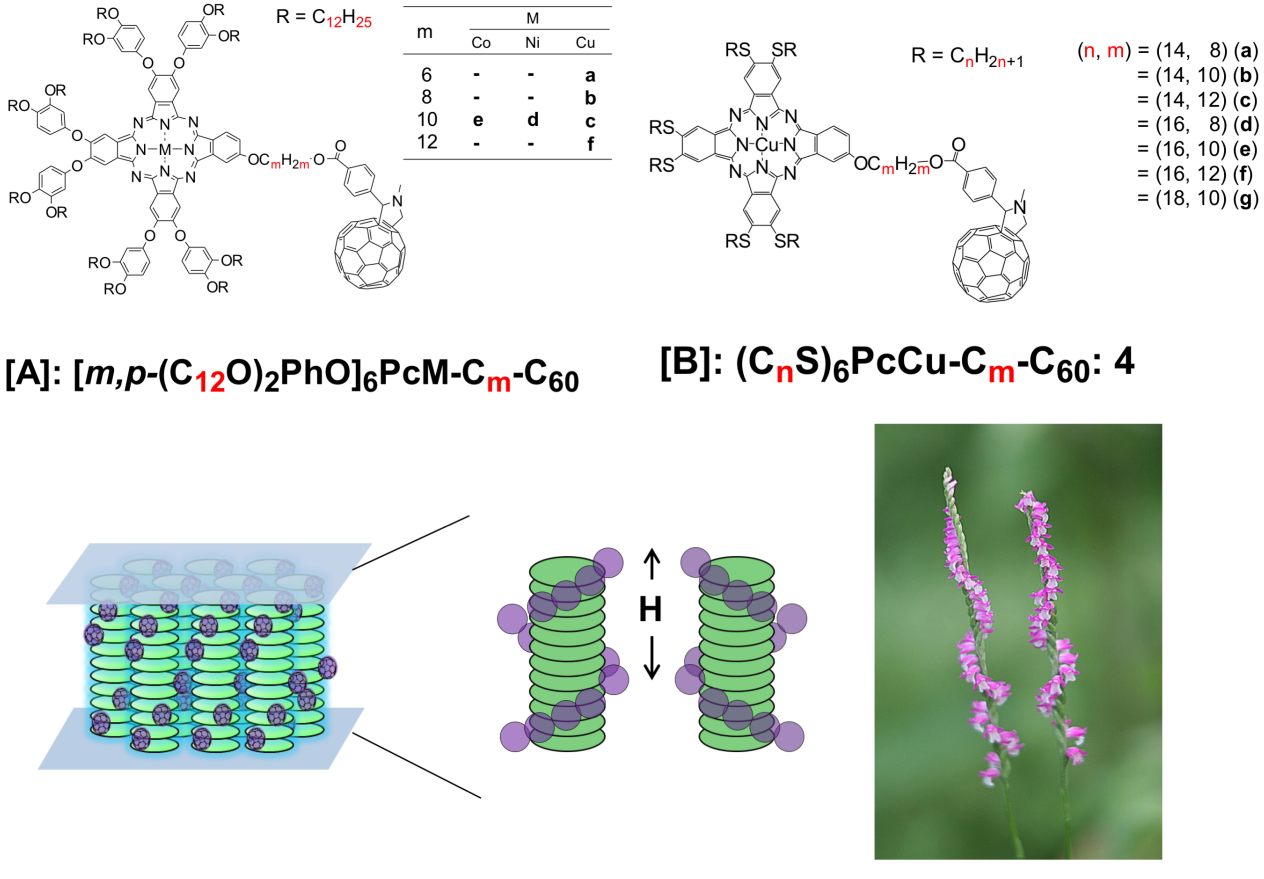

Fig. 1. Liquid crystalline PcM-C_{60} dyads showing spiranthes-like supramolecular structure in homeotropic alignment

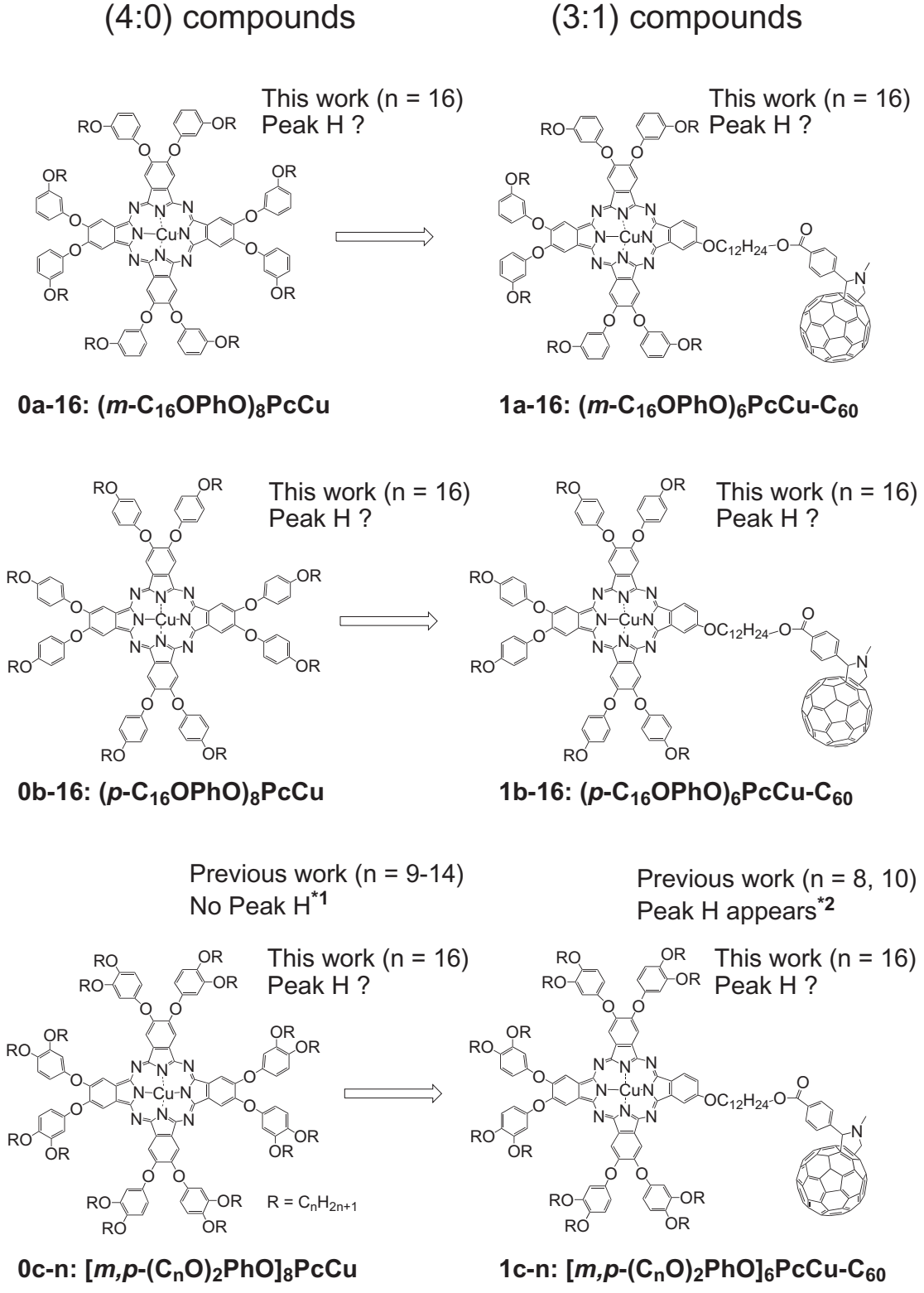

Fig. 2. Dependence of the substitution position of alkoxy chains on appearance of the helical pitch H of fullerene moieties in columnar structure. *1: Ref. 28; *2: Refs. 5 and 21

Therefore, we are very interested in the influence of the substitution position of alkoxy chains on homeotropic alignment and appearance of the helical supramolecular structure (Peak H). In this work, we planned to synthesize three different $(PhO)_6PcCu\text{-}C_{60}$-based dyads: the *m-substituted* derivative **1a-16**, the *p-substituted* derivative **1b-16** and the *m,p-substituted* derivative **1c-16**, as illustrated in Fig. 2. For easy

comparison, the length of the chain (R=C_nH_{2n+1}) is fixed to n = 16 and we have prepared the parent (4:0) compounds {**0a~0c-16**} and their corresponding children (3:1) compounds: the OH-substituted compounds {**3a~3c-16**}, OFBA-substituted compounds {**2a~2c-16**} and the C_{60}-substituted compounds {**1a~1c-16**}. The letters of **a**, **b** and **c** with the entry numbers mean the *m-substituted* derivative, *p-substituted* derivative and *m,p-substituted* derivative, respectively. For these twelve novel Pc compounds, we have investigated the influence of both substitution position of the alkoxy chains and the type of terminal groups (OH, OFBA and C_{60}) on the mesomorphism, the homeotropic alignment, the stacking distance h and appearance of the helical supramolecular structure (Peak H).

EXPERIMENTAL

Synthesis

The syntheses of this study were carried out with reference to our previously reported methods [20, 21, 28–30], as illustrated in Scheme 1. The detailed procedures are described in the following.

12-*Bromododecan*-1-*ol* (6). To a three-necked flask were added dry toluene (52 mL), dodecane-1,12-diol (3.49 g, 17.2 mmol) and 46% aqueous solution of HBr (2.4 mL). The reaction mixture was heated at 120 °C for 48 h with stirring under a nitrogen atmosphere. Then it was extracted with ethyl acetate and washed with brine. The organic layer was dried over Na_2SO_4 overnight and evaporated *in vacuo*. The residue was purified by column chromatography (silica gel, *n*-hexane : ethyl acetate = 3 : 2, R_f = 0.58) to afford 2.45 g of white solid. Yield: 53.5%. Mp: 29.8 °C.

4-(12-*Hydroxydodecyoxy*)*phthalonitrile* (4). To a three-necked flask were added dry DMF (24 mL), 4-hydroxyphthalonitrIile (0.627 g, 4.43 mmol), K_2CO_3 (1.0 g) and 12-bromododecan-1-ol (**6**: 1.52 g, 5.72 mmol). The reaction mixture was heated at 100 °C for 1 h with stirring under a nitrogen atmosphere. Then it was extracted with chloroform and washed with brine. The organic layer was dried over Na_2SO_4 overnight and evaporated *in vacuo.* The residue was purified by column chromatography (silica gel, chloroform: ethyl acetate = 4 : 1, R_f = 0.48) to give 0.597 g of white solid. Yield: 82.6%. Mp: 69.5 °C (lit.: 69.7 °C [20]).

^{1}H-NMR (400 Mhz; $CDCl_3$; TMS): δ, ppm 1.20–1.84 (20 H, m), 3.64 (2H, dd, J_1 = 12.0 Hz, J_2 = 6.4 Hz, -OCH$_2$CH_2-), 4.04 (2H, t, J = 6.6 Hz, -OCH_2-), 7.17 (1 H, dd, J = 8.6 Hz, J = 2.6 Hz, Ar-*H*), 7.25 (1H, d, J = 2.4 Hz, Ar-*H*), 7.69 (1 H, d, J = 9.2 Hz, Ar-*H*).

3-*Hexadecylphenol* (7). To a three-necked flask were added dry DMF (50 mL), resorcinol (6.14 g, 0.0560 mol), 1-bromohexadecane (17.7 g, 0.058 mol) and K_2CO_3

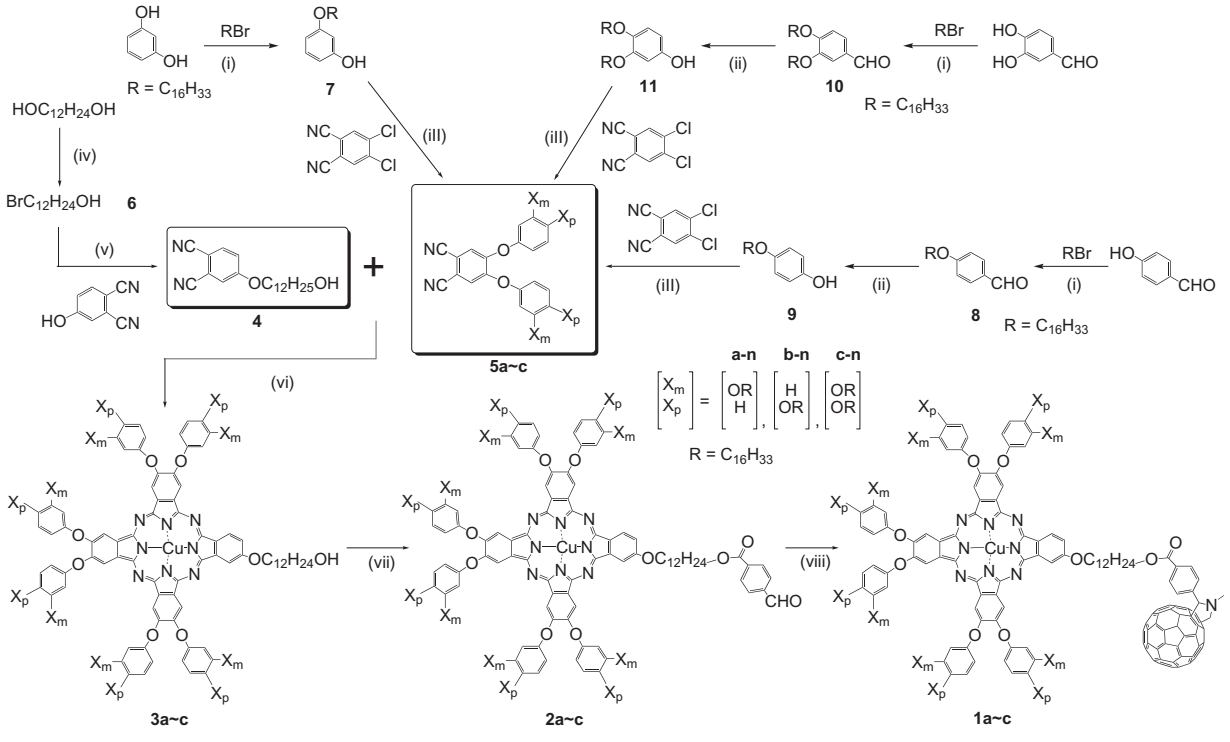

Scheme 1. Synthetic route of (***m*-C_{16}OPhO)$_6$PcCu-C_{60} (1a-16)**, (***p*-C_{16}OPhO)$_6$PcCu-C_{60} (1b-16)** and **[*m*,*p*-(C_{16}O)$_2$PhO]$_6$PcCu-C_{60} (1c-16)**. (i) RBr/K_2CO_3/DMA; (ii) conc.H_2SO_4, 30% H_2O_2 aq., $CHCl_3$, MeOH; (iii) K_2CO_3/DMA; (iv) 46% HBr aq./Toluene; (v) K_2CO_3/DMF; (vi) DBU, 1-Hexanol, $CuCl_2$; (vii) 4-Formylbenzoic acid, DCC, DMAP, CH_2Cl_2; (viii) *N*-Methylglycine, C_{60}, Toluene

(8.30 g). The reaction mixture was heated at 100 °C for 1 h with stirring under a nitrogen atmosphere. Then it was extracted with chloroform and washed with brine. The organic layer was dried over Na_2SO_4 and evaporated *in vacuo*. The residue was purified by column chromatography (silica gel, chloroform, R_f = 0.24) to afford 3.30 g of white solid. Yield: 17.0%. Mp: 63.0 °C.

^{1}H-NMR (400 Mhz; $CDCl_3$; TMS): δ, ppm 0.88 (3H, t, J = 7.2 Hz, -CH_3), 1.21–1.47 (26H, m), 1.73–1.80 (2H, m), 3.92 (2H, t, J = 6.4 Hz, -OCH_2-), 4.71 (1H, s, -O*H*), 6.38–6.50 (3H, m, Ar-*H*), 7.09–7.13 (1H, m, Ar-*H*).

4-(*Hexadecyloxy*)*benzaldehyde* (8). To a three-necked flask were added dry DMF (60 mL), 4-hydroxybenzaldehyde (3.00 g, 24.6 mmol), 1-bromohexadecane (8.23 g, 27.0 mmol) and K_2CO_3 (2.22 g). The reaction mixture was refluxed for 2 h with stirring under a nitrogen atmosphere. Then it was extracted with chloroform and washed with water. The organic layer was dried over Na_2SO_4 and evaporated *in vacuo*. The residue was purified by column chromatography (silica gel, chloroform, R_f = 0.48) to give 6.50 g of white solid. Yield: 76.1%. Mp: 43.6 °C.

^{1}H-NMR (400 Mhz; $CDCl_3$; TMS): δ, ppm 0.90 (3H, t, J = 6.4 Hz, -CH_3), 1.23–1.52 (26H, m), 1.79–1.87 (2H, m), 4.02 (2H, t, J = 6.4 Hz), 6.99–7.05 (2H, m, Ar-*H*), 7.83–7.87 (2H, m, Ar-*H*), 9.90 (1H, s, -C*H*O).

4-(*Hexadecyloxy*)*phenol* (9). A mixture of chloroform (60 mL), 4-(hexadecyloxy)benzaldehyde (**8**: 4:07 g, 11.5 mmol), 30% H_2O_2 aq (9.8 g), H_2SO_4 (15 drops) and methanol (43 mL) was added to an Erlenmeyer flask and stirred at room temperature for 46 h with blocking out of the light. The reaction mixture was extracted with chloroform and washed with brine. The organic layer was dried over Na_2SO_4 and evaporated *in vacuo*. The residue was purified by column chromatography (silica gel 150 g, chloroform, R_f = 0.18) to afford 2.07 g of white solid. Yield: 53.6%. Mp: 86.2 °C.

^{1}H-NMR (CD_3SO; TMS): δ, ppm 0.85 (3H, t, J = 6.8 Hz, -CH_3), 1.19–1.42 (26H, m), 1.61–1.68 (2H, m), 3.82 (2H, t, J = 6.8 Hz), 6.62–6.74 (2H, m), 8.86 (1H, s, -O*H*).

3,4-*Bis(hexadecyloxy)benzaldehyde* (10). To a three-necked flask were added dry DMF (20 mL), 3,4-dihydroxybenzaldehyde (3.04 g, 0.0220 mol), 1-bromohexadecane (13.9 g, 0.0456 mol) and K_2CO_3 (3.04 g). The reaction mixture was stirred at room temperature for 10 min under N_2 gas atmosphere, and then refluxed for 1 h with stirring. It was checked by TLC (silica gel, chloroform) and found the starting material of 3,4-dihydroxybenzaldehyde. Accordingly, 1-bromohexadecane (6.91 g, 0.0226 mol) was added to the reaction mixture. Since the starting material disappeared after 4 h, the reaction mixture was extracted with chloroform and washed with water three times. The organic layer was dried over Na_2SO_4 overnight and then evaporated *in vacuo*. The residue was purified by column chromatography (silica gel, chloroform, R_f = 0.58) to afford 10.3 g of white solid. Yield: 79.6%. Mp: 80.4 °C.

^{1}H-NMR (400 MHz; $CDCl_3$; TMS): δ, ppm 0.81 (6H, t, J = 6.4 Hz, -CH_3), 1.13–1.46 (52H, m), 1.78 (4H, sextet, J = 6.8 Hz), 3.96–4:02 (4H, m), 6.88 (1 H, d, J = 8.4 Hz, Ar-*H*), 7.33–7.36 (2H, m, Ar-*H*), 9.76 (1H, s, -C*H*O).

3,4-*Bis*(*hexadecyloxy*)*phenol* (11). A mixture of chloroform (20 mL), 3,4-bis(hexadecyloxy)benzaldehyde (**10**: 4.62 g, 0.00787 mmol), 30% H_2O_2 aq (8.5 g), H_2SO_4 (10 drops) and methanol (31 mL) was added to an Erlenmeyer flask and stirred at room temperature for 24 h with blocking out of the light. Then the reaction mixture was extracted with chloroform and washed with brine three times. The organic layer was dried over Na_2SO_4 and evaporated *in vacuo*. The residue was recrystallized from *n*-hexane to give 3.54 g of white solid. Yield: 80.1%. Mp: 94.1 °C.

^{1}H-NMR (400 MHz; $CDCl_3$; TMS): δ, ppm 0.91 (6H, t, J = 6.4 Hz, -CH_3), 1.23–1.52 (53H, m), 1.74–1.86 (4H, m), 3.91–3.99 (4H, m), 6.32 (1H, dd, J_1 = 2.8, J_2 = 8.4 Hz, Ar-*H*), 6.47 (1H, d, J = 2.8 Hz, Ar-*H*), 6.78 (1H, d, J = 8.4 Hz, Ar-*H*), 9.76 (s, -O*H*).

4,5-*Bis*(3-(*hexadecyloxy*)*phenoxy*)*phthalonitrile* (5a). To a three-necked flask were added dry DMA (10 mL), 3-(hexadecyloxy)phenol (**7**: 1.50 g, 4.49 mmol), 4,5-dichlorophthalonitrile (0.381 g, 1.93 mmol) and K_2CO_3 (1.4 g). The reaction mixture was heated at 130 °C for 2 h with stirring under nitrogen atmosphere. Then it was extracted with chloroform and washed with brine. The organic layer was dried over Na_2SO_4 overnight and evaporated *in vacuo*. The residue was purified by column chromatography (silica gel, chloroform, R_f = 0.71) to afford 1.00 g of white solid. Yield: 65.3%. Mp: 73.5 °C (lit; 73.2 °C [21]).

^{1}H-NMR (400 MHz; $CDCl_3$; TMS): δ, ppm 0.88 (3H, t, J = 6.4 Hz, -CH_3), 1.20–1.49 (26H, m), 1.75–1.82 (2H, m), 3.95 (2H, t, J = 6.4 Hz, -OCH_2-), 6.60–6.82 (6H, m, Ar-*H*), 7.20 (2H, s, Ar-*H*), 7.32 (2H, t, J = 8.0 Hz, Ar-*H*).

4,5-*Bis*(4-(*hexadecyloxy*)*phenoxy*)*phthalonitrile*) (5b). To a three-necked flask were added dry DMA (20 mL), 4-(hexadecyloxy)phenol (**9**: 1.80 g, 5.38 mmol), 4,5-dichlorophthalonitrile (0.528 g, 1.9 mmol) and K_2CO_3 (1.4 g). The reaction mixture was refluxed for 30 min with stirring under a nitrogen atmosphere. Then it was extracted with chloroform and washed with brine. The organic layer was dried over Na_2SO_4 overnight and evaporated *in vacuo*. The residue was recrystallized from ethanol to give 1.86 g of white solid. Yield: 87.6%. Mp: 106.1 °C.

^{1}H-NMR (400 MHz; $CDCl_3$; TMS): δ, ppm 0.88 (6H, t, J = 6.8 Hz, -CH_3), 1.13–1.51 (52H, m), 1.81 (4H, quint, -CH_2-), 3.98 (4H, t, J = 6.4 Hz, -O-CH_2-), 6.95–7.05 (10H, m, Ar-*H*).

4,5-*Bis*(3,4-*bis*(*hexadecyloxy*)*phenoxy*)*phthalonitrile* (5c). To a three-necked flask were added dry DMA (20 mL), 4,5-dichlorophthalonitrile (157.7 mg, 0.800 mol), 3,4-bis(hexadecyloxy)phenol (**11**: 1.00 g, 1.74 mmol) and K_2CO_3 (3.49 g). The reaction mixture

was stirred at room temperature for 10 min and then refluxed for 2 h with stirring under a nitrogen atmosphere. It was extracted with chloroform and washed with brine. The organic layer was dried over Na_2SO_4 overnight and evaporated *in vacuo*. The residue was purified by column chromatography (silica gel, chloroform, R_f = 0.71) to afford 655.2 mg of white solid. Yield: 64.2%. Mp: 96.2 °C.

^{1}H-NMR (400 MHz; $CDCl_3$; TMS): δ, ppm 0.81 (12 H, t, J = 6.4 Hz, -CH_3), 1.19–1.43 (104 H, m), 1.72–1.79 (8 H, m), 3.89 (4H, t, J = 6.4 Hz), 3.95 (4H, t, J = 6.4 Hz, -OCH_2-), 6.52–6.59 (4H, m, Ar-*H*), 6.84 (2H, d, J = 8.8 Hz, Ar-*H*), 7.02 (2H, s, Ar-*H*).

***(m-C$_{16}$OPhO)$_6$PcCu-OH* (3a-16).** To a three-necked flask were added 1-hexanol (30 mL), 4-(12-hydroxydodecyoxy)phthalonitrile (**4**: 0.108 g, 0.327 mmol), 4,5-bis(3-(hexadecyloxy)phenoxy)phthalonitrile (**5a**: 0.731 g, 0.922 mmol) and $CuCl_2$ (0.0512 g, 0.0381 mmol). The reaction mixture was stirred at room temperature for 10 min and then DBU (3 drops) was added. It was heated at 160 °C for 24 h with stirring under a nitrogen atmosphere. After cooling to room temperature, methanol was poured into the reaction mixture to precipitate the target compound. The precipitate was collected by filtration, washed with methanol, ethanol and acetone successively. Chloroform was added, and the solvent was then evaporated *in vacuo*. The residue was purified by column chromatography (silica gel, chloroform) to remove a by-product of the (4:0) parent PcCu compound (**0a-16**: R_f = 1.00) and collected the (3:1) target PcCu compound (**3a-16**: R_f = 0.34). After removal of the solvent, 237.9 mg of green solid was obtained in yield 18.0%.

Elemental analysis and MALDI-TOF mass data: See Table 1.

UV-vis spectral data: See Table 2.

Phase transition behavior: See Table 3.

***(p-C$_{16}$OPhO)$_6$PcCu-OH* (3b-16).** To a three-necked flask were added 1-hexanol (60 mL), 4-(12-hydroxydodecyoxy)phthalonitrile (**4**: 0.209 g, 0.636 mmol), 4,5-bis-(4-(hexadecyloxy)phenoxy)phthalonitrile (**5b**: 1.04 g, 1.77 mmol) and $CuCl_2$ (0.108 g, 0.803 mmol). The reaction mixture was stirred at room temperature for 10 min and then DBU (3 drops) was added. It was heated at 160 °C for 24 h with stirring under a nitrogen atmosphere. After cooling to room temperature, methanol was poured into the reaction mixture to precipitate the target compound. The precipitate was collected by filtration, washed with methanol, ethanol and acetone successively. Chloroform was added, and the solvent was then evaporated *in vacuo*. The residue was purified by column chromatography (silica gel, chloroform) to remove a by-product of the (4:0) parent PcCu compound (**0b-16**: R_f = 1.00) and to collect the (3:1) target PcCu compound (**3b-16**: R_f = 0.18). After removal of the solvent, 346 mg of green solid was obtained in yield 20.5%.

Elemental analysis and MALDI-TOF mass data: See Table 1.

UV-vis spectral data: See Table 2.

Phase transition behavior: See Table 3.

***(m,p-C$_{16}$OPhO)$_6$PcCu-OH* (3c-16).** To a three-necked flask were added 1-hexanol (15 mL), 4-(12-hydroxydodecyoxy)phthalonitrile (**4**: 0.606 g, 0.476 mmol), 4,5-bis-(4-(hexadecyloxy)phenoxy)phthalonitrile (**5c**: 0.055 g, 0.167 mol), and $CuCl_2$ (29.2 mg, 0.217 mmol). The reaction mixture was stirred at room temperature for 10 min and then DBU (3 drops) was added. It was heated at 160 °C for 20 h with stirring under a nitrogen atmosphere. After cooling to room temperature, methanol was poured into the reaction mixture to precipitate the target compound. The precipitate was collected by filtration, washed with methanol, ethanol and acetone successively. Chloroform was added, and the solvent was then evaporated *in vacuo*. The residue was purified by column chromatography (silica gel, toluene) to remove a by-product of the (4:0) parent PcCu compound (**0c-16**: R_f = 1.00) and collected the (3:1) target PcCu compound (**3c-16**: R_f = 0.70). After removal of the solvent, 243 mg of green solid was obtained in yield 34.1%.

Elemental analysis and MALDI-TOF mass data: See Table 1.

UV-vis spectral data: See Table 2.

Phase transition behavior: See Table 3.

***(m-C$_{16}$OPhO)$_6$PcCu-OFBA* (2a-16).** To a three-necked flask were added dry 1,2-dichloroethane (20 mL), (*m*-C_{16}OPhO)$_6$PcCu-OH (**3a-16**: 0.153 g, 0.0555 mmol), 4-formylbenzoic acid (0.0165 g, 0.110 mmol), DMAP (0.0473 g, 0.387 mmol) and DCC (0.143 g, 0.6952 mmol). The reaction mixture was refluxed with stirring for 45 h under a nitrogen atmosphere. After cooling to room temperature, methanol was poured into the reaction mixture to precipitate the target compound. The precipitate was collected by filtration, washed with methanol, ethanol and acetone successively. Chloroform was added, and the solvent was then evaporated *in vacuo*. The residue was purified by column chromatography (silica gel, chloroform, R_f = 0.78) to afford 0.0259 g of green solid in yield 16.1%.

Elemental analysis and MALDI-TOF mass data: See Table 1.

UV-vis spectral data: See Table 2.

Phase transition behavior: See Table 3.

***(p-C$_{16}$OPhO)$_6$PcCu-OFBA* (2b-16).** To a three-necked flask were added dry toluene (20 mL), (*p*-C_{16}OPhO)$_6$-PcCu-OH (**3b-16**: 0.142 g, 0.0513 mmol), 4-formylbenzoic acid (0.0154 g, 0.103 mmol), DMAP (0.0250 g, 0.205 mmol) and DCC (0.106 g, 0.0513 mmol). The reaction mixture was stirred at room temperature for 3 h and then refluxed with stirring for 24 h under a nitrogen gas atmosphere. After cooling to room temperature, methanol was poured into the reaction mixture to precipitate the target compound. The precipitate was collected by filtration, washed with methanol, ethanol and acetone successively. Chloroform was added, and the solvent was then evaporated *in vacuo*. The residue was purified by column chromatography (silica gel, chloroform: dichloromethane = 1:1, R_f = 0.78) to afford 163.0 mg of green solid in yield 75.4%.

Table 1. MALDI-TOF mass spectral data, elemental analysis data and yields of **3a~3c-16**, **2a~2c-16**, **1a~1c-16** and **0a~0c-16**

Compound	Mol. formula (Mol. wt)	Exact mass	Observed exact mass	Elemental analysis: Found (%) (Calcd.) (%)			Yield (%)
				C	H	N	
3a-16: (*m*-C_{16}OPhO)$_6$PcCu-OH	$C_{176}H_{256}N_8O_{14}Cu$ (2771.51)	2768.886	2769.072	76.60 (76.27)	9.65 (9.31)	3.89 (4.04)	18.0
3b-16: (*p*-C_{16}OPhO)$_6$PcCu-OH	$C_{176}H_{256}N_8O_{14}Cu$ (2771.51)	2768.886	2768.651	76.34 (76.27)	9.68 (9.31)	4.05 (4.04)	20.5
3c-16: [*m*,*p*-(C_{16}O)$_2$PhO]$_6$PcCu-OH	$C_{272}H_{448}CuN_8O_{20}$ (4214.06)	4210.358	4210.574	77.74 (77.52)	10.74 (10.72)	3.06 (2.66)	34.1
2a-16: (*m*-C_{16}OPhO)$_6$PcCu-OFBA	$C_{184}H_{260}N_8O_{16}Cu$ (2903.62)	2900.907	2901.146 (M+H)	76.34 (76.11)	9.13 (9.03)	3.69 (3.86)	16.1
2b-16: (*p*-C_{16}OPhO)$_6$PcCu-OFBA	$C_{184}H_{260}N_8O_{16}Cu$ (2903.62)	2900.907	2900.553	76.45 (76.11)	9.43 (9.03)	3.89 (3.86)	75.4
2c-16: [*m*,*p*-(C_{16}O)$_2$PhO]$_6$PcCu-OFBA	$C_{280}H_{452}CuN_8O_{22}$ (4346.17)	4342.379	4342.843	77.26 (77.38)	10.54 (10.48)	2.18 (2.58)	56.6
1a-16: (*m*-C_{16}OPhO)$_6$PcCu-C_{60}	$C_{246}H_{265}N_9O_{15}Cu$ (3651.33)	3648.962 (M+H)	3649.153 (M+H)	—	—	—	20.2
1b-16: (*p*-C_{16}OPhO)$_6$PcCu-C_{60}	$C_{246}H_{265}N_9O_{15}Cu$ (3651.33)	3648.962 (M+H)	3649.180 (M+H)	—	—	—	63.1
1c-16: [*m*,*p*-(C_{16}O)$_2$PhO]$_6$PcCu-C_{60}	$C_{342}H_{457}N_9O_{21}Cu$ (5093.88)	5089.426	5089.399	—	—	—	34.1
0a-16: (*m*-C_{16}OPhO)$_8$PcCu*[1]	$C_{208}H_{304}N_8O_{16}Cu$ (3236.23)	3233.26	3236.23	76.87 (77.20)	9.76 (9.47)	3.86 (3.46)	
0b-16: (*p*-C_{16}OPhO)$_8$PcCu	$C_{208}H_{304}N_8O_{16}Cu$ (3236.23)	3233.251	3233.249	77.16 (77.20)	9.65 (9.47)	3.41 (3.46)	
0c-16: (*m*,*p*-(C_{16}O)$_2$PhO]$_8$PcCu	$C_{336}H_{560}N_8O_{24}Cu$ (5159.63)	5156.221 (M+H)	5156.486 (M+H)	77.98 (78.21)	11.03 (10.94)	2.07 (2.17)	

*Ref. 30.

Table 2. UV-vis spectral data in $CHCl_3$ of **3a~3c-16**, **2a~2c-16**, **1a~1c-16** and **0a~0c-16**

Compound	Concentration[#] ($\times 10^{-6}$ mol/L)	λ_{max} (nm) (logε)						
		C_{60} Peak	Soret-band			Q_{0-1}	Aggr.	Q_{0-0}
3a-16: (*m*-C_{16}OPhO)$_6$PcCu-OH	9.73		282.6 (4.77)	341.3 (4.82)	394.8 (4.40)	614.5 (4.57)	*ca.* 647 (sh)	683.6 (5.20)
3b-16: (*p*-C_{16}OPhO)$_6$PcCu-OH	2.98		291.6 (4.80)	338.7 (4.87)	392.9 (4.41)	614.3 (4.62)	*ca.* 650 (sh)	683.1 (5.31)
3c-16: [*m*,*p*-(C_{16}O)$_2$PhO]$_6$PcCu-OH	5.93		291.4 (4.84)	340.3 (4.87)	397.7 (4.40)	614.9 (4.55)	*ca.* 654 (sh)	684.1 (5.26)
2a-16: (*m*-C_{16}OPhO)$_6$PcCu-OFBA	3.10		283.5 (4.81)	340.8 (4.89)	394.4 (4.46)	614.7 (4.63)	*ca.* 649 (sh)	683.4 (5.30)
2b-16: (*p*-C_{16}OPhO)$_6$PcCu-OFBA	3.24		291.2 (4.86)	338.4 (4.91)	395.1 (4.48)	614.3 (4.66)	*ca.* 650 (sh)	683.1 (5.33)
2c-16: [*m*,*p*-(C_{16}O)$_2$PhO]$_6$PcCu-OFBA	5.77		288.8 (4.84)	340.5 (4.82)	396.8 (4.42)	615.3 (4.51)	*ca.* 653 (sh)	685.2 (5.21)
1a-16: (*m*-C_{16}OPhO)$_6$PcCu-C_{60}	5.47	254.4 (4.93)		336.9 (4.72)	393.1 (4.28)	616.0 (4.34)	*ca.* 649 (sh)	682.9 (4.91)
1b-16: (*p*-C_{16}OPhO)$_6$PcCu-C_{60}	5.12	253.0 (5.13)	288.1 (5.04)	338.7 (4.94)	397.4 (4.47)	621-658 (4.7)		683.1 (5.08)
1c-16: [*m*,*p*-(C_{16}O)$_2$PhO]$_6$PcCu-C_{60}	6.19	255.1 (5.21)	289.7 (5.07)	336.6 (4.96)	397.9 (4.47)	616.9 (4.52)	*ca.* 653 (sh)	685.2 (5.12)
0a-16: (*m*-C_{16}OPhO)$_8$PcCu	2.30		283.8 (4.85)	340.8 (4.92)	395.0 (4.51)	614.5 (4.57)	650.9 (4.61)	682.4 (5.41)
0b-16: (*p*-C_{16}OPhO)$_8$PcCu	3.13		290.6 (4.89)	339.8 (4.82)	408.9 (5.39)	614.3 (4.50)	649.8 (4.48)	683.1 (5.21)
0c-16: (*m*,*p*-(C_{16}O)$_2$PhO]$_8$PcCu	2.47		290.7 (4.87)	338.5 (4.74)	381.3 (4.44)	613.7 (4.37)	648.4 (4.29)	683.1 (4.96)

[#]: In chloroform; Aggr.: Aggregation band of Q_{0-0} band; sh: Shoulder.

Table 3. Phase transition temperatures and enthalpy changes of **0a~0c-16**, **3a~3c-16**, **2a~2c-16** and **1a~1c-16**

Compound	Phase	T/°C [ΔH(kJmol^{-1})]	Phase
0a-16: (*m*-C_{16}OPhO)$_8$PcCu*1	K	34.5 [64.8] ⇄	Col$_{ho}$	160.9 [18.0] ⇄	I.L.
0b-16: (*p*-C_{16}OPhO)$_8$PcCu	K	116.0[157.2] →	Col$_{hd}$	266.5[7.15] ⇄	I.L.
0c-16: [*m,p*-(C_{16}O)$_2$PhO]$_8$PcCu	K	55.6 [126.9] ⇄	Col$_{hd}$	117.2 [95.3] ⇄	Col$_{tet.d}$	163.8 [2.15] ⇄	I.L.
3a-16: (*m*-C_{16}OPhO)$_6$PcCu-OH	Col$_{ho1}$	83.4 [0.368] ⇄	Col$_{ho2}$	157.6 [17.6] ⇄	Col$_{ho3}$	201.4 [8.31] ⇄	I.L.
3b-16: (*p*-C_{16}OPhO)$_6$PcCu-OH	K_{1v}	34.1 [73.2] →	Col$_{ho}$	235.5 [6.69] ⇄	I.L.
	K_{2v}	56.1 →			
	K_{3v}	86.5[8.55] ⇄			
3c-16: [*m,p*-(C_{16}O)$_2$PhO]$_6$PcCu-OH	K	52.6 [205.4] ⇄	Col$_{hd}$	121.6 [22.3] ⇄	Col$_{tet.d}$	148.3 [1.57] ⇄	I.L.
2a-16: (*m*-C_{16}OPhO)$_6$PcCu-OFBA	Col$_{ho1}$	157.3 [22.8] ⇄	Col$_{ho2}$	193.2 [14.2] ⇄	I.L.
2b-16: (*p*-C_{16}OPhO)$_6$PcCu-OFBA	K	92.3 [10.9] →	Col$_{ho}$	245.7 [6.00] ⇄	I.L.
2c-16: [*m,p*-(C_{16}O)$_2$PhO]$_6$PcCu-OFBA	K	72.6[197.4] ⇄	Col$_{hd}$	94.7[42.1] ⇄	I.L.
1a-16: (*m*-C_{16}OPhO)$_6$PcCu-C_{60}	Col$_{ho}$	148.0 [24.8] ⇄	I.L.
1b-16: (*p*-C_{16}OPhO)$_6$PcCu-C_{60}	K	84.7 [1.47] →	Col$_{ho}$	139.1 [3.79] ⇄	I.L.
1c-16: [*m,p*-(C_{16}O)$_2$PhO]$_6$PcCu-C_{60}	K	59.8 [220.3] →	Col$_{hd}$	93.8 [31.8] ⇄	I.L.

*Phase nomenclature: K = crystal, Col$_{ho}$ = hexagonal ordered columnar mesophase, Col$_{hd}$ = hexagonal disordered columnar mesophase, Col$_{tet.o}$ = tetragonal ordered columnar mesophase, Col$_{tet.d}$ = tetragonal disrodered columnar mesophase, Col$_{ro}$ = rectangular ordered columnar mesophase, and I.L, = isotropic liquid, v = virgin sample. ▭ = mesophase showing homeotropic alignment.
*1: Ref. 31.

Elemental analysis and MALDI-TOF mass data: See Table 1.

UV-vis spectral data: See Table 2.

Phase transition behavior: See Table 3.

***(m,p-C$_{16}$OPhO)$_6$PcCu-OFBA* (2c-16).** To a three-necked flask were added dry toluene (20 mL), (*m,p*-C_{16}OPhO)$_6$PcCu-OH (**3c-16**: 0.143 g, 0.0339 mmol), 4-formylbenzoic acid (11.2 mg, 0.0746 mmol), DMAP (18.7 mg, 0.153 mmol) and DCC (71.4 mg, 0.346 mmol). The reaction mixture was stirred at room temperature for 3 h under a nitrogen atmosphere. It was checked by TLC (silica gel, chloroform) and the starting material of (*m,p*-C_{16}OPhO)$_6$PcCu-OH (**3c-16**) was found. Accordingly, 4-formylbenzoic acid (29.9 mg, 0.199 mmol), DMAP (49.1 mg, 0.4:02 mmol) and DCC (132.6 mg, 0.643 mmol) were added and it was refluxed for an additional 5 h with

stirring under a nitrogen atmosphere. After cooling to room temperature, methanol was poured into the reaction mixture to precipitate the target compound. The precipitate was collected by filtration, washed with methanol, ethanol and acetone successively. Chloroform was added, and the solvent was then evaporated *in vacuo*. The residue was purified by column chromatography (silica gel 140 g, chloroform : toluene = 1:1, R_f = 0.83) to afford 83.3 mg of green solid in yield 56.6%.

Elemental analysis and MALDI-TOF mass data: see Table 1.

UV-vis spectral data: See Table 2.

Phase transition behavior: See Table 3.

(*m*-C_{16}*OPhO*)$_6$*PcCu*-C_{60} (1a-16). To a three-necked flask were added dry toluene (40 mL), (*m*-C_{16}OPhO)$_6$PcCu-OFBA (**2a-16**: 80.8 mg, 0.0278 mmol), fullerene (40.9 mg, 0.0568 mmol) and *N*-methylglycine (6.0 mg, 0.0673 mmol). The reaction mixture was refluxed for 12 h with stirring under a nitrogen atmosphere. After cooling to room temperature, methanol was poured into the reaction mixture to precipitate the target compound. The precipitate was collected by filtration, washed with methanol, ethanol and acetone successively. Chloroform was added, and the solvent was then evaporated *in vacuo*. The residue was purified by column chromatography (silica gel 100 g, chloroform: *n*-hexane = 2 : 5, R_f = 0.93) and then by HPLC (Japan Analytical Industry Co. Ltd. LC-918) to afford 20.8 mg of green solid in yield 20.2%.

Elemental analysis and MALDI-TOF mass data: See Table 1.

UV-vis spectral data: See Table 2.

Phase transition behavior: See Table 3.

(*p*-C_{16}*OPhO*)$_6$*PcCu*-C_{60} (1b-16). To a three-necked flask were added dry toluene (20 mL), (*p*-C_{16}OPhO)$_6$PcCu-OFBA (**2b-16**: 73.2 mg, 0.0252 mmol), fullerene (37.3 mg, 0.0518 mmol) and *N*-methylglycine (5.7 mg, 0.0640 mmol). The reaction mixture was refluxed for 16 h with stirring under a nitrogen atmosphere. After cooling to room temperature, methanol was poured into the reaction mixture to precipitate the target compound. The precipitate was collected by filtration, washed with methanol, ethanol and acetone successively. Chloroform was added, and the solvent was then evaporated *in vacuo*. The residue was purified by column chromatography (silica gel 100 g, chloroform : *n*-hexane = 2 : 5, R_f = 0.65) and then by HPLC (Japan Analytical Industry Co. Ltd. LC-918) to afford 58.1 mg of green solid in yield 63.1%.

Elemental analysis and MALDI-TOF mass data: See Table 1.

UV-vis spectral data: See Table 2.

Phase transition behavior: See Table 3.

(*m,p*-C_{16}*OPhO*)$_6$*PcCu*-C_{60} (1c-16). To a three-necked flask were added dry toluene (20 mL), (*m,p*-C_{16}OPhO)$_6$-PcCu-OFBA (**2c-16**: 42.2 mg, 0.00970 mmol), fullerene (14.1 mg, 0.0196 mmol) and *N*-methylglycine (2.8 mg, 0.0314 mmol). The reaction mixture was refluxed for 24 h with stirring under a nitrogen atmosphere. After cooling to room temperature, the solvent was evaporated *in vacuo*. The residue was purified by column chromatography (Silica gel 100 g, chloroform, R_f = 0.95) and then by HPLC (Japan Analytical Industry Co. Ltd. LC-918) to afford 16.8 mg of green solid in yield 34.1%.

Elemental analysis and MALDI-TOF mass data: See Table 1.

UV-vis spectral data: See Table 2.

Phase transition behavior: See Table 3.

Measurements

HPLC was carried out by using an LC-9110 NEXT recycling preparative from Japan Analytical Industry Co. Ltd. The infrared absorption spectra were recorded by using a Nicolet NEXUS 670 FT-IR spectrometer. The ^{1}H-NMR measurements were carried out by using a Bruker Ultrashield 400 MHz. The elemental analyses were performed by using a Perkin–Elmer Elemental Analyzer 2400. The MALDI-TOF mass spectral measurements were carried out by using a Bruker Daltonics Autoflex III spectrometer (matrix: dithranol). Table 1 summarizes the elemental analysis and MALDI-TOF mass data. Electronic absorption (UV-vis) spectra were recorded by using a Hitachi U-4100 spectrophotometer. Table 2 summarizes these UV-vis spectral data. Phase transition behavior of the present compounds was observed with a polarizing optical microscope (Nikon ECLIPSE E600 POL) equipped with a Mettler FP82HT hot stage and a Mettler FP90 Central Processor, and a Shimadzu DSC-50 differential scanning calorimeter. The mesophases were identified by using a small angle X-ray diffractometer (Bruker Mac SAXS System) equipped with a temperature-variable sample holder adapted from a Mettler FP82HT hot stage. The phase transition temperatures and the transition enthalpy changes are listed in Table 3. Figs. 3 and 4 illustrate the setup of the SAXS system and the setup of the temperature-variable sample holder, respectively. As can be seen from Fig. 3, the generated X-ray is bent by two convergence monochrometers to produce a point X-ray beam (diameter = 1.0 mm). The point beam runs through the holes of the temperature-variable sample holder. As illustrated in Fig. 4, into the temperature-variable sample holder of Mettler FP82HT hot stage, a glass plate (76 mm × 19 mm × 1.0 mm) with a hole (diameter = 1.5 mm) is inserted. The hole can be charged with a powder sample (*ca*. 1 mg). The measurable range is from 3.0 Å to 110 Å and the temperature range is from room temperature to 375 °C. This SAXS system is available for all condensed phases including the fluid nematic phase and isotropic liquid.

RESULTS AND DISCUSSION

Synthesis

Table 1 lists MALDI-TOF mass and the elemental analysis data for all the PcCu products. As can be seen from this table, the observed values agree well with

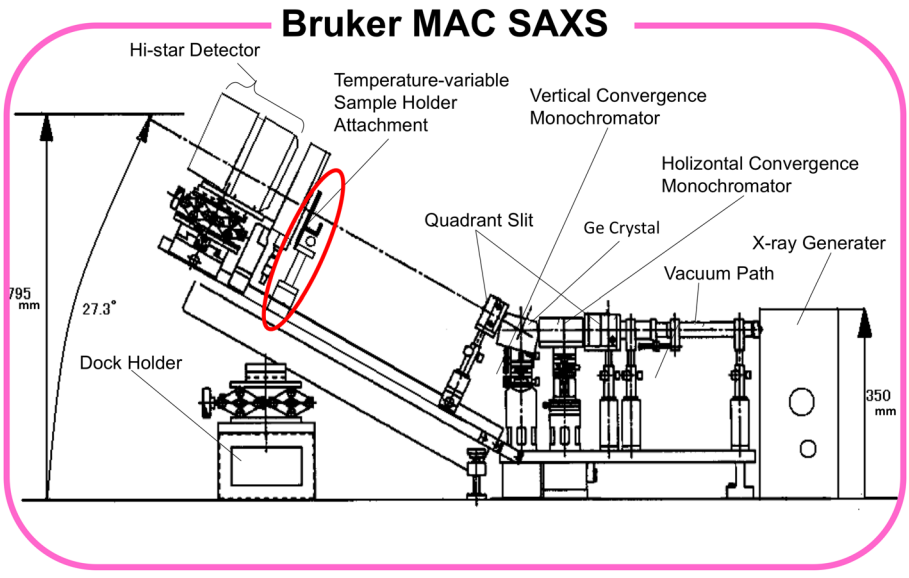

Fig. 3. Setup of small angle X-ray scattering (SAXS) apparatus equipped with a temperature-variable sample holder

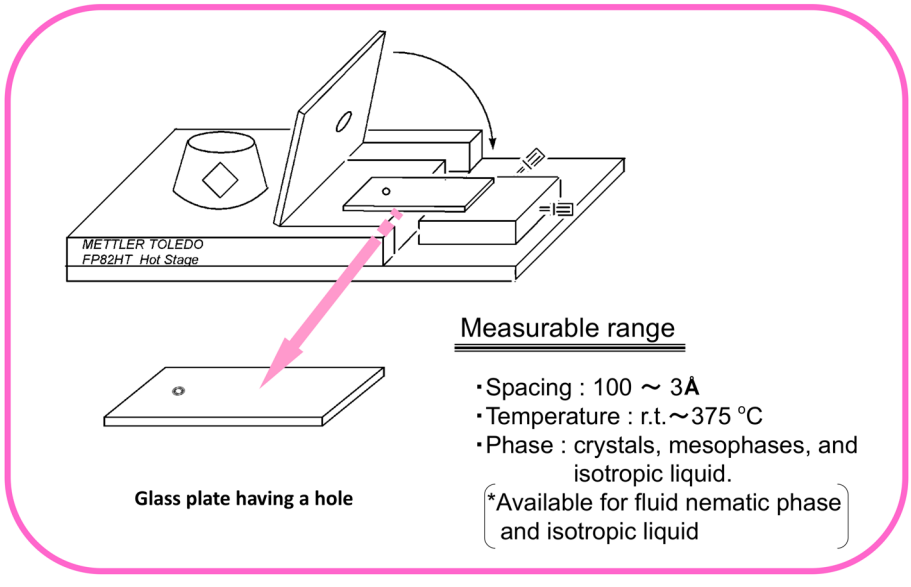

Fig. 4. Setup of the temperature-variable sample holder

the theoretical values for both the TOF mass and the elemental analyses for all the PcCu products, so that it was confirmed that all the target products were successfully synthesized. The $(PhO)_6PcCu\text{-}C_{60}$ dyads **1a~1c-16** were not completely combustible so that the element analyses could not be effective. However, it was confirmed from the MALDI-TOF mass spectra and ultraviolet-visible absorption spectra that the $(PhO)_6PcCu\text{-}C_{60}$ dyads **1a~1c-16** were successfully synthesized. As can be seen from Table 2, each of the $(PhO)_6PcCu\text{-}C_{60}$ dyads **1a~1c-16** gives both the $Q_{0\text{-}0}$ band around 683 nm characteristic to PcCu having D_{4h} symmetry and the band at 253–255 nm due to fullerene (C_{60}). From these results, we could judge that the target $(PhO)_6PcCu\text{-}C_{60}$ dyads **1a~1c-16** were certainly synthesized.

Phase transition behavior

Table 3 shows the phase transition behavior of the parent (4:0) compounds {**0a~0c-16**} and their corresponding children (3:1) compounds: the OH-substituted compounds {**3a~3c-16**}, OFBA-substituted compounds {**2a~2c-16**} and the C_{60}-substituted compounds {**1a~1c-16**}. The detailed phase transitions will be explained below.

(4:0) ***Compounds*** **{0a~0c-16}.** As can be seen from Table 3, the *m-substituted* derivative **0a-16** and the *p-substituted* derivative **0b-16** showed only one columnar liquid crystalline phase, Col_{ho} and Col_{hd}, respectively. The Col_{ho} phase of the *p-substituted* derivative **0b-16** cleared into an isotropic liquid at 266.5 °C. This cp

was much higher than those of the *m-substituted* derivative **0a-16** and the *m,p-substituted* derivative **0c-16**. Unlike the *m-substituted* derivative **0a-16** and the *p-substituted* derivative **0b-16**, the *m,p-substituted* derivative **0c-16** showed two kinds of columnar liquid crystalline phases, Col_{hd} and $Col_{tet,d}$. More interestingly, this high temperature mesophase $Col_{tet.d}$ showed perfect homeotropic alignment between two glass plates (see Fig. 5.) A similar homeotropic alignment was also observed for the $Col_{tet.d}$ phases in the homologues **0c–0n** (n = 11–14) having different alkoxy chain length [28].

***OH-substituted compounds* {3a~3c-16}.** As can be seen from Table 3, the *m-substituted* derivative **3a-16** is liquid crystalline at room temperature and showed three different Col_{ho} phases from Col_{ho1}, Col_{ho2} and Col_{ho3}. On the other hand, the *p-substituted* derivative **3b-16** is crystalline at room temperature and shows a mixture of three crystalline polymorphs K_1, K_2 and K_3 as the virgin state. Upon heating, each of the crystalline phases melted into a Col_{ho} mesophase; on further heating, it cleared into an isotropic liquid (I.L.) at a high temperature of 235.5 °C. The cp (235.5 °C) of this *p-substituted* derivative **3b-16** is much higher than those of the *m-substituted* derivative **3a-16** and the *m,p-substituted* derivative **3c-16**. The *m,p-substituted* **3c-16** shows two different mesophases, Col_{hd} and $Col_{tet.d}$, and the high temperature mesophase $Col_{tet.d}$ shows perfect homeotropic alignment between two glass plates (see Fig. 5). Thus, the mesomorphism of the *m,p-substituted* derivative **3c-16** is exactly the same as that of the corresponding parent (4:0) compound **0c-16**.

***OFBA-substituted compounds* {2a~2c-16}.** As can be seen from Table 3, the *m-substituted* derivative **2a-16** shows a Col_{ho1} mesophase at room temperature. On heating from room temperature, it transformed into another Col_{ho2} mesophase and then into an isotropic liquid (I.L.). On the other hand, the *p-substituted* derivative **2b-16** is crystalline at room temperature. On heating, the crystalline *K* phase melts into a Col_{ho} phase and then clears into an I.L. at a high temperature of 245.7 °C, which is much higher than those of the other derivatives of *m-substituted* **2a-16** and *m,p-substituted* **2c-16**. The *m,p-substituted* derivative **2c-16** is also crystalline (K) at room temperature, like the *m-substituted* derivative **2a-16**. It melts into a Col_{hd} phase at 59.8 °C. The Col_{hd}

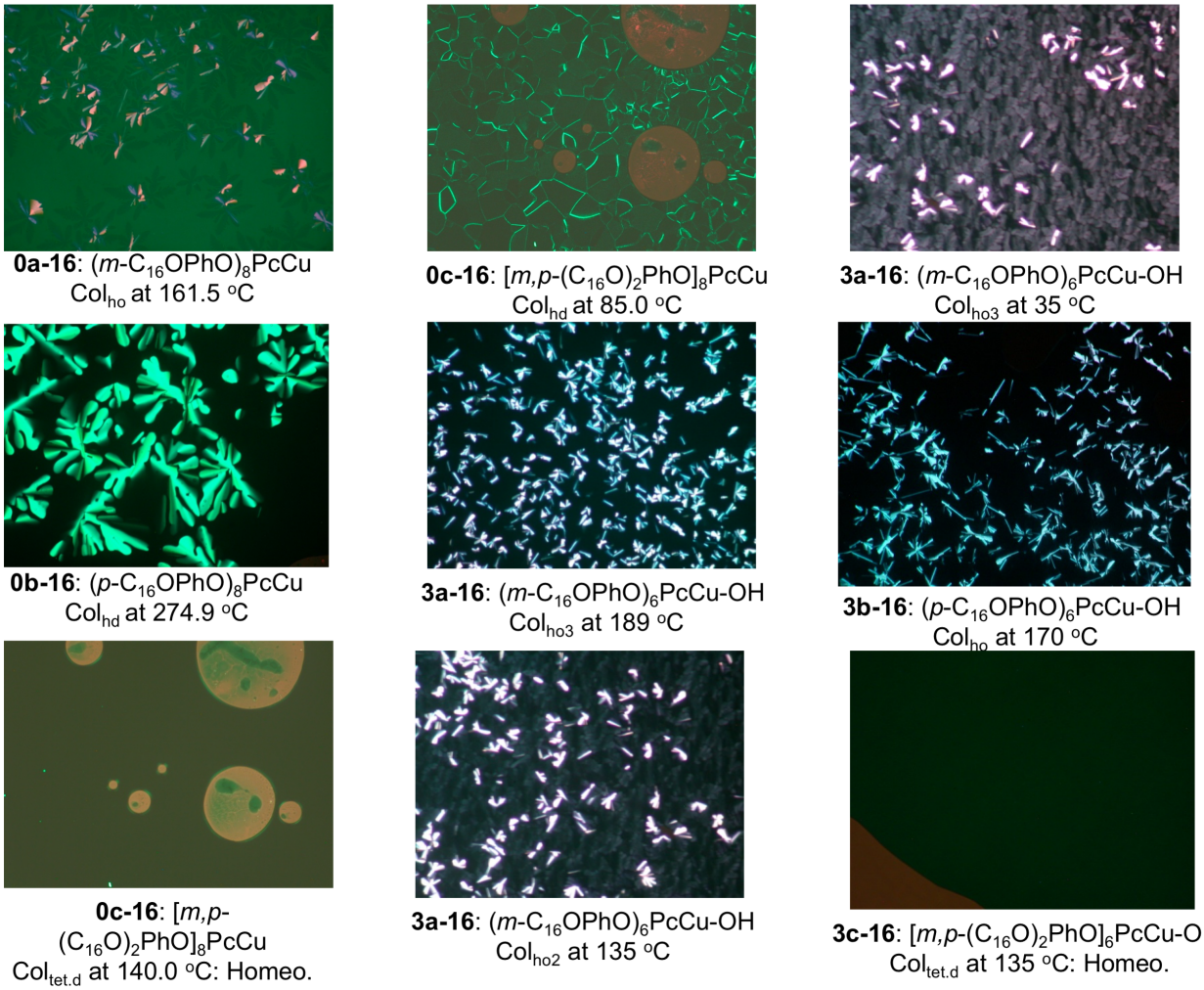

Fig. 5. Photomicrographs of the phthalocyanine-based liquid crystals, **0a~0c-16**, **3a~3c-16**, **2a~2c-16** and **1a~1c-16**

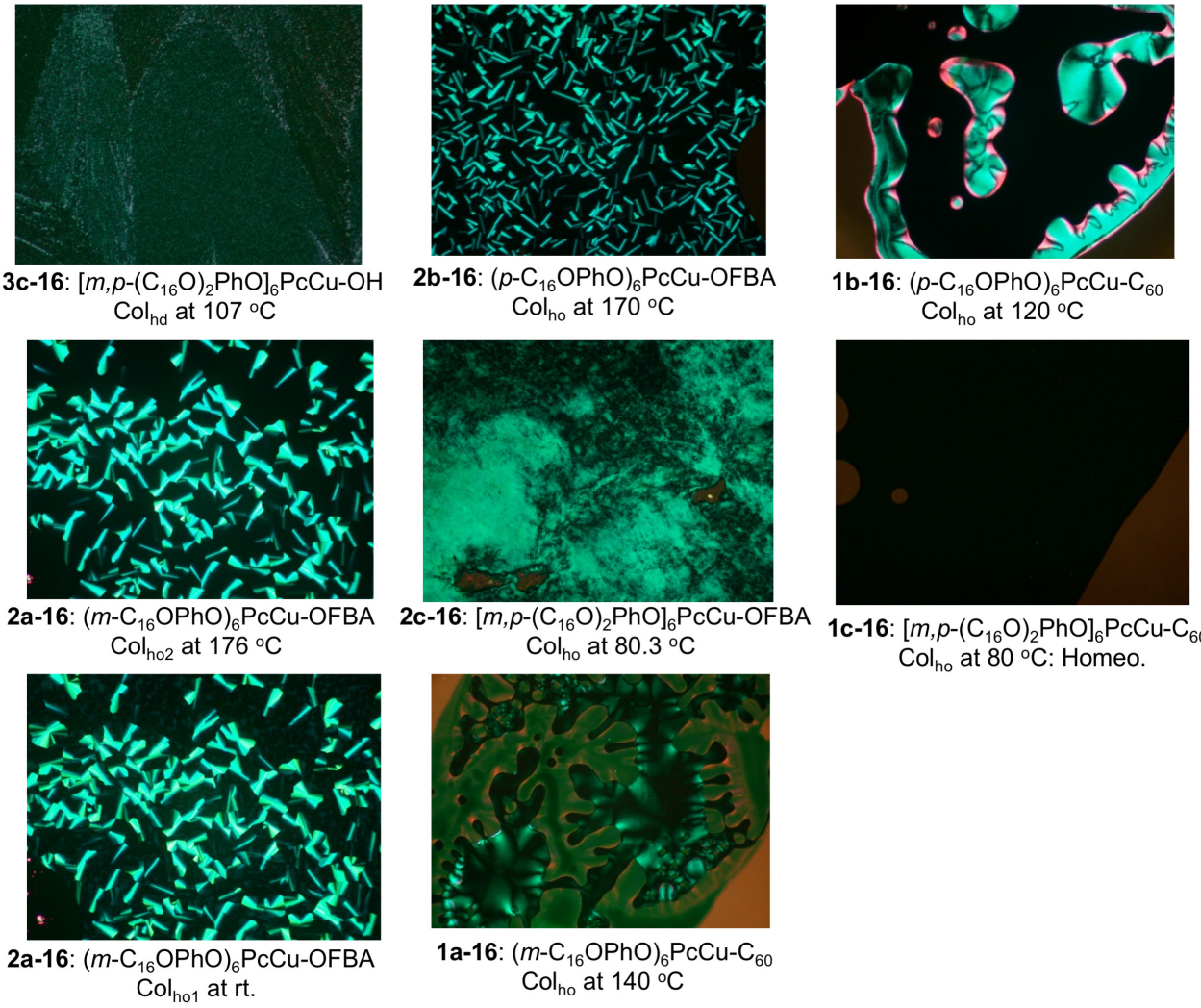

Fig. 5. (*Continued*)

phase of **2c-16** did not show homeotropic alignment, unlike the corresponding parent (4:0) compound **0c-16** and the precursor **3c-16** (see Fig. 5).

***C_{60}-substituted compounds* {1a~1c-16}.** As shown in Table 3, the *m-substituted* derivative **1a-16** exhibits a Col_{ho} mesophase at room temperature. When heated it cleared into an I.L. On the other hand, the *p-substituted* derivative **1b-16** exhibits a crystal (*K*) at room temperature. When heated, it melts into the Col_{ho} phase and then clears into an I.L. When this I.L. was cooled down to room temperature, it remained in the Col_{ho} phase without recrystallization. The *m,p-substituted* derivative **1c-16** was in a crystalline phase (K) at room temperature, like the *p-substituted* derivative **1b-16**. On heating from room temperature, it melted into the Col_{hd} phase and then cleared into I.L. When this I.L. was cooled down to room temperature, it remained in the Col_{hd} phase without recrystallization. This Col_{hd} mesophase showed perfect homeotropic alignment between two glass plates (see Fig. 5). Thus, in the C_{60}-substituted compounds {**1a~1c-16**} the *m,p-substituted* derivative **1c-16** only shows homeotropic alignment, whereas neither the *m-substituted* derivative **1a-16** nor the *p-substituted* derivative **1b-16** shows homeotropic alignment. It is noteworthy that the same tendency could be also observed in the parent (4:0) compounds and the OH-substituted compounds (see Fig. 5).

The homeotropic alignment of *m,p-substituted* **1c-16** was proved as shown in Fig. 6. A small amount of the derivative **1c-16** was first sandwiched between two glass plates and heated up over the cp to completely clear into an isotropic liquid. The I.L. was cooled to 90 °C in the Col_{hd} mesophase temperature range to obtain perfect homeotropic alignment. The cover slip was removed at this temperature, and the thin film was scratched with a spatula or something like a needle. Figure 6 shows a photomicrograph of the scratched sample between crossed polarizers. As you can see from this photomicrograph, only the scratched parts show birefringence while the other parts are completely dark. As illustrated in the

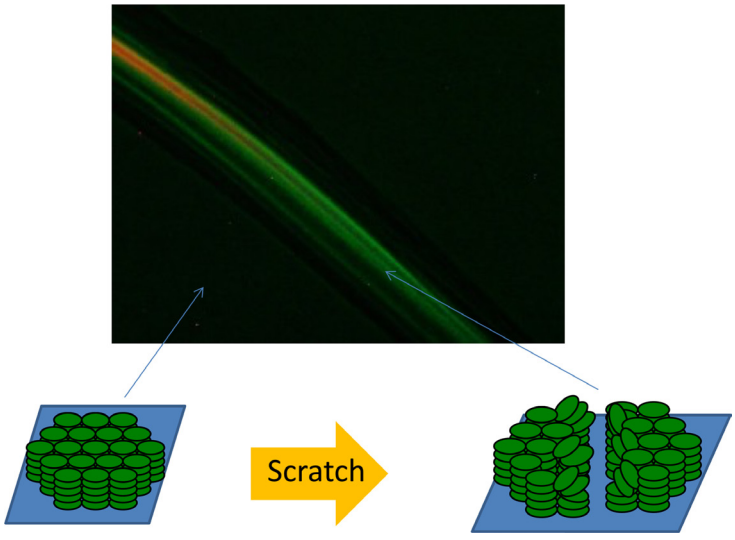

Fig. 6. Photomicrograph of the Col_{ho} mesophase of (***m,p*-C_{16}OPhO)$_6$PcCu-C_{60} (1c-16**) at 90 °C showing homeotropic alignment. The dark area showed homeotropic alignment but the scratched part turned to show birefringence

figure, the columns are vertically oriented with respect to the substrate in the homeotropic parts, so that the parts give darkness under crossed Nicols. When you scratch this thin film with a needle, birefringence will appear due to the collapse of the vertically oriented columns to show blight parts. In the case of isotropic liquid or Cub phase, such birefringence does not appear. From these microscopic observations, it was proven that the *m,p-substituted* derivative **1c-16** was homeotropically aligned.

Thus, only the *m,p-substituted* derivative **1c-16** exhibited homeotropic alignment in the (PhO)$_6$PcCu-C_{60}-based complexes, and neither the *m-substituted* derivative **1a-16** nor a *p-substituted* derivative **1b-16** showed homeotropic alignment. Therefore, large doubt remains for the homeotropic alignment of the *p-substituted* derivative (*p*-C_{12}OPhO)$_6$PcZn-OPh-C_{60} (= PcZn-C_{60}) reported by another research group [10, 15, 16, 26]. The homeotropic alignment in their *p-substituted* derivative should be proven by the above-described method using a polarization microscope.

Temperature-variable small angle X-ray diffraction studies

Figure 7 illustrates three different measurement methods for temperature-variable small angle X-ray diffraction:

Method A: non-aligned sample;

Method B: homogeneously aligned sample of ordered columns between two glass plates;

Method C: homeotropically aligned sample of ordered columns between two glass plates.

In Method A, polydomain of liquid crystalline phase is filled into a hole. In this case, the reflections both from 2D and 1D lattices can be observed. In Method B, a homogeneously aligned sample gives the reflections only from the 1D lattice in the *Z*-direction. In Method C, a homeotropically aligned sample gives the reflections only from the 2D lattice in the XY plane. If the peak H were a periodicity along the *Z*-axis direction of column, the peak H should disappear for the homeotropically aligned sample in Method C [21].

Therefore, at first, it was investigated using Method A whether or not each of the liquid crystalline phases was identified and Peak H corresponding to the pitch of the helix appeared. Figures 8, 9, 10 and 11 show X-ray diffraction patterns of the parent (4:0) compounds {**0a~0c-16**}, the OH-substituted compounds {**3a~3c-16**}, the OFBA-substituted compounds {**2a~2c-16**} and the C_{60}-substituted compounds {**1a~1c-16**}, respectively. All the X-ray data are summarized in Table 4. The detailed XRD results will be explained below.

(4:0) *Compounds* {0a~0c-16}. As can be seen from Fig. 8, the *m-substituted* parent (4:0) compound **0a-16** shows three peaks from No. 1 to No. 3 in the low angle region, and two peaks, No. 4 and No. 5, in the high angle region, for the liquid crystalline phase at 100 °C. As can be seen from Table 4, these three peaks in the low angle region were well assigned to (100), (110) and (200) reflections from a 2D hexagonal lattice. A broad peak No. 4 is attributed to a halo due to the molten alkyl groups. Peak No. 5 was attributable to a (001) reflection corresponding to stacking between Pc disks in the columns. Therefore, this liquid crystal phase could be identified as a hexagonal ordered columnar (Col_{ho}) phase. From these assignments, the lattice constant a = 43.2 Å of the 2D hexagonal lattice and the stacking distance h = 3.39 Å were obtained. Assuming that the density of the liquid crystalline phase was 1.0 g·cm^3, the number of molecules per unit lattice (Z) was calculated to be just 1.0. This Z value is consistent with a Col_{ho} phase [31].

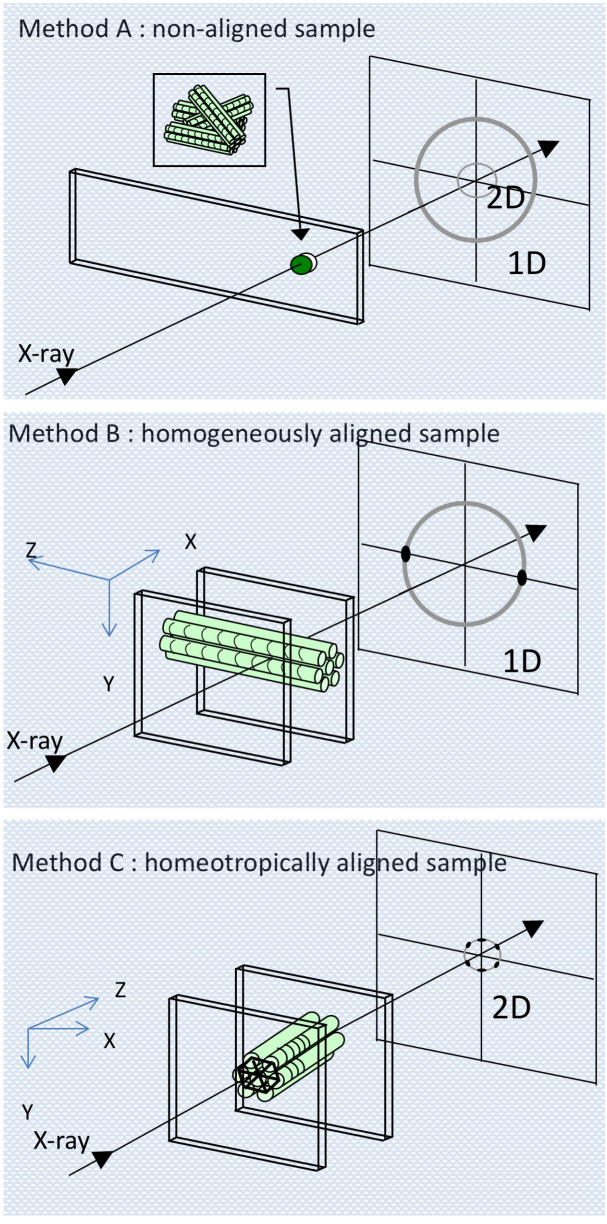

Fig. 7. Illustration of X-ray photographs of Method A: non-aligned sample; Method B: homogeneously aligned sample; Method C: homeotropically aligned sample of ordered columns between two glass plates. In Method A, polydomain of liquid crystalline phase is filled into a hole. In this case, the reflections both from 2D and 1D lattices can be observed. In Method B, homogeneously aligned sample gives the reflections only from 1D lattice in Z-direction. In Method C, homeotropically aligned sample gives the reflections only from 2D lattice in XY plane. If the peak H would be a periodicity along the *Z* axis direction of column, the peak H should disappear for the homeotropically aligned sample in Method C. Ref. 21

In the same manner, all the other mesophases in the *p-substituted* derivative **0b-16** and the *m,p-substituted* derivative **0c-16** could be identified as Col_{hd} (for **0b-16**), Col_{hd} and $Col_{tet.d}$ (for **0c-16**), respectively.

As can be seen from Fig. 8, the mesophases in *p-substituted* derivative **0b-16** and *m,p-substituted* derivative **0c-16** gave no reflection around $2\theta = 26^{o}$ corresponding to the stacking distance (h) between Pc disks in the columns, unlike the mesophase of *m-substituted* derivative **0a-16**. Also, each of the parent (4:0) compounds {**0a~0c-16**} gave no Peak H due to the helical supramolecular structure around $2\theta = 1.0$.

***OH-substituted compounds* {3a~3c-16}.** As shown in Fig. 9, the X-ray diffraction patterns of three mesophases in the *m-substituted* derivative **3a-16** were measured at room temperature, 130 °C and 180 °C. Several diffraction peaks attributable to reflection from the 2D hexagonal lattice could be observed, commonly in the low angle region. When the biggest peak in the lowest angle region was assumed as the (001) reflection from a 2D hexagonal lattice, all the peaks could be well assigned as the reflections from the 2D hexagonal lattice. On the other hand, the peak in the highest angle region could be assigned as the (001) reflection corresponding to stacking between Pc disks in the columns. Therefore, all these three mesophases could be identified as Col_{ho1}, Col_{ho2} and Col_{ho3}. As can be seen from Table 4, when the density of these mesophases Col_{ho1}, Col_{ho2} and Col_{ho3} are assumed to be 0.97, 0.95, and 0.90 $g \cdot cm^{-3}$, respectively, the number of molecules Z per unit lattice is just 1.0. The *Z* value is compatible to a Col_{ho} phase [31].

Figure 9 also shows the X-ray diffraction pattern of the Col_{ho} mesophase in the *p-substituted* derivative **3b-16** at 160 °C. As can be seen from the XRD pattern, Peak No. 4 of the (001) reflection corresponding to stacking distance *h* in the highest angle region was considerably broader compared to that of the *m-substituted* derivative **3b-16**. Also, as can be seen from Table 4, when the density of this mesophase is assumed to be 0.90 $g \cdot cm^{-3}$, the number of molecules *Z* per unit lattice is just 1.0. This Z value is consistent with the Col_{ho} phase [31].

As can also be seen from Fig. 9, the X-ray diffraction patterns of the mesophases at 100 °C and 134 °C in the *m,p-substituted* derivative **3c-16** gave no (001) reflection peak corresponding to stacking in the highest angle region, unlike the *m-substituted* derivative **3a-16** and the *p-substituted* derivative **3b-16**. As can be seen from Table 4, these two mesophases of the *m,p-substituted* derivative **3c-16** could be identified as Col_{hd} and $Col_{tet.d,}$ similarly to the corresponding *m,p-substituted* parent (4:0) compound **0c-16**.

Furthermore, it is apparent from Fig. 9 that each of the OH-substituted compounds {**3a~3c-16**} gave no Peak H due to the helical supramolecular structure around $2\theta =$ 1.0, similarly to the parent (4:0) compounds {**0a~0c-16**}.

***OFBA-substituted compounds* {2a~2c-16}.** In Fig. 10 are shown the X-ray diffraction patterns of the *m-substituted* derivative **2a-16** at room temperature and 175 °C. As can be seen from this figure, each of these two mesophases gave several diffraction peaks attributable to reflections from a 2D hexagonal lattice in the low angle

Table 4. X-ray data of the mesophases in **0a~0c-16**, **3a~3c-16**, **2a~2c-16** and **1a~1c-16**

Compound (mesophase)	Lattice constants/Å	Peak no.	Spacing/Å		Miller indices (*h k l*)
			Observed	Calculated	
0a-16: (*m*-C_{16}OPhO)$_8$PcCu	a = 43.2	1	37.4	37.4	(1 0 0)
(Col_{ho} at 100 °C)	h = 3.39	2	21.9	21.6	(1 1 0)
	Z = 1.0 for ρ = 1.0	3	19.0	18.7	(2 0 0)
		4	*ca.* 4.7	—	#
		5	3.39	3.39	(0 0 1)[h]
0b-16: (*p*-C_{16}OPhO)$_8$PcCu	a = 41.5	1	35.9	35.9	(1 0 0)
(Col_{hd} at 207 °C)		2	19.7	20.7	(1 1 0)
		3	*ca.* 5.0	—	#
0c-16: [*m*,*p*-(C_{16}O)$_2$PhO]$_8$PcCu	a = 48.6	1	42.1	42.1	(1 0 0)
(Col_{hd} at 86 °C)		2	24.3	24.0	(1 1 0)
		3	*ca.* 9.2	9.19	(4 1 0)
		4	*ca.* 4.6	—	#
($Col_{tet.d}$ at 135 °C)	a = 34.5	1	34.5	34.5	(1 1 0)
		2	24.7	24.4	(2 0 0)
		3	*ca.* 9.7	9.6	(3 2 0)
		4	*ca.* 4.8	—	#
3a-16: (*m*-C_{16}OPhO)$_6$PcCu-OH	a = 40.2	1	34.8	34.8	(1 0 0)
(Col_{ho1} at rt)	h = 3.44	2	19.8	20.1	(1 1 0)
	Z = 1.0 for ρ = 0.97	3	17.3	17.4	(2 0 0)
		4	12.9	13.2	(2 1 0)
		5	9.79	9.65	(3 1 0)
		6	8.61	8.70	(4 0 0)
		7	*ca.* 4.6	—	#
		8	3.44	—	(0 0 1)[h]
(Col_{ho2} at 130 °C)	a = 40.8	1	35.3	35.3	(1 0 0)
	h = 3.46	2	20.3	20.4	(1 1 0)
	Z = 1.0 for ρ = 0.95	3	17.5	17.7	(2 0 0)
		4	9.68	9.79	(3 1 0)
		5	*ca.* 4.8	—	#
		6	3.46	—	(0 0 1)[h]
(Col_{ho3} at 180 °C)	a = 41.0	1	35.5	35.5	(1 0 0)
	h = 3.43	2	20.4	20.5	(1 1 0)
	Z = 1.0 for ρ = 0.90	3	17.6	17.7	(2 0 0)
		4	*ca.* 4.8	—	#
		5	3.43	—	(0 0 1)[h]
3b-16: (*p*-C_{16}OPhO)$_6$PcCu-OH	a = 41.5	1	35.9	35.9	(1 0 0)
(Col_{ho} at 160 °C)	h = 3.50	2	20.2	20.7	(1 1 0)
	Z = 1.0 for ρ = 0.90	3	*ca.* 4.9	—	#
		4	3.50	—	(0 0 1)[h]
3c-16: (*m*,*p*-C_{16}OPhO)$_6$PcCu-OH	a = 47.2	1	40.9	40.9	(1 0 0)
(Col_{hd} at 100 °C)		2	23.0	23.6	(1 1 0)
		3	14.9	15.5	(2 1 0)
		4	10.7	10.2	(4 0 0)
		5	8.85	8.93	(4 1 0)
		6	*ca.* 4.6	—	#

(*Continued*)

Table 4. (*Continued*)

Compound (mesophase)	Lattice constants/Å	Peak no.	Spacing/Å		Miller indices (*h k l*)
			Observed	Calculated	
($Col_{tet.d}$ at 134 °C)	a = 33.2	1	33.2	33.2	(1 0 0)
		2	24.9	23.5	(1 1 0)
		3	9.60	9.21	(3 2 0)
		4	*ca*. 4.7	—	#
2a-16: (*m*-C_{16}OPhO)$_6$PcCu-OFBA	a = 41.5	1	35.9	35.9	(1 0 0)
(Col_{ho1} at rt)	h = 3.49	2	20.8	20.7	(1 1 0)
	Z = 1.0 for ρ = 0.95	3	18.2	18.0	(2 0 0)
		4	9.76	9.96	(3 1 0)
		5	*ca*. 4.7	—	#
		6	3.49	3.49	(0 0 1)[h]
(Col_{ho2} at 175 °C)	a = 44.0	1	38.1	38.1	(1 0 0)
	h = 3.47	2	21.9	22.0	(1 1 0)
	Z = 1.0 for ρ = 0.85	3	19.3	19.1	(2 0 0)
		4	14.2	14.4	(2 1 0)
		5	9.60	9.52	(4 0 0)
		6	*ca*. 4.9	—	#
		7	3.47	3.47	(0 0 1)[h]
2b-16: (*p*-C_{16}OPhO)$_6$PcCu-OFBA	a = 42.5	1	36.8	36.8	(1 0 0)
(Col_{ho} at 169 °C)	h = 3.49	2	20.4	21.2	(1 1 0)
	Z = 1.0 for ρ = 0.90	3	17.1	18.4	(2 0 0)
		4	13.3	13.9	(2 1 0)
		5	*ca*. 4.9	—	#
		6	3.49	3.49	(0 0 1)[h]
2c-16: [*m*,*p*-(C_{16}O)$_2$PhO]$_6$PcCu-OFBA	a = 40.5	1	35.1	35.9	(1 0 0)
(Col_{hd} at 120 °C)		2	19.6	20.7	(1 1 0)
		3	10.2	10.1	(2 2 0)
		4	*ca*. 4.8	—	#
1a-16: (*m*-C_{16}OPhO)$_6$PcCu-C_{60}	H = 69.2	1	69.0	—	H
(Col_{ho} at 120 °C)	a = 40.2	2	34.8	34.8	(1 0 0)
	h = 3.46	3	19.9	20.1	(1 1 0)
	Z = 1.0 for ρ = 1.3	4	*ca*. 9.0	8.70	(4 0 0)
		5	*ca*. 4.7	—	#
		6	3.46	3.46	(0 0 1)[h]
1b-16: (*p*-C_{16}OPhO)$_6$PcCu-C_{60}	a = 40.2	1	34.8	34.8	(1 0 0)
(Col_{ho} at 100 °C)	h = 3.37	2	19.3	20.1	(1 1 0)
	Z = 1.0 for ρ = 1.3	3	*ca*. 4.7	—	#
		4	3.37	3.37	(0 0 1)[h]
1c-16: [*m*,*p*-(C_{16}O)$_2$PhO]$_6$PcCu-C_{60}	a = 43.6	1	80.3	—	H
(Col_{ho} at 90 °C)		2	37.8	37.8	(1 0 0)
		3	20.4	21.8	(1 1 0)
		4	10.2	10.5	(3 1 0)
		5	*ca*. 4.7	—	#

= Halo of the molten alkyl chain, h = Stacking distance between the monomers. H = Helical pitch of the fullerences; ρ: assumed density (g/cm^3).

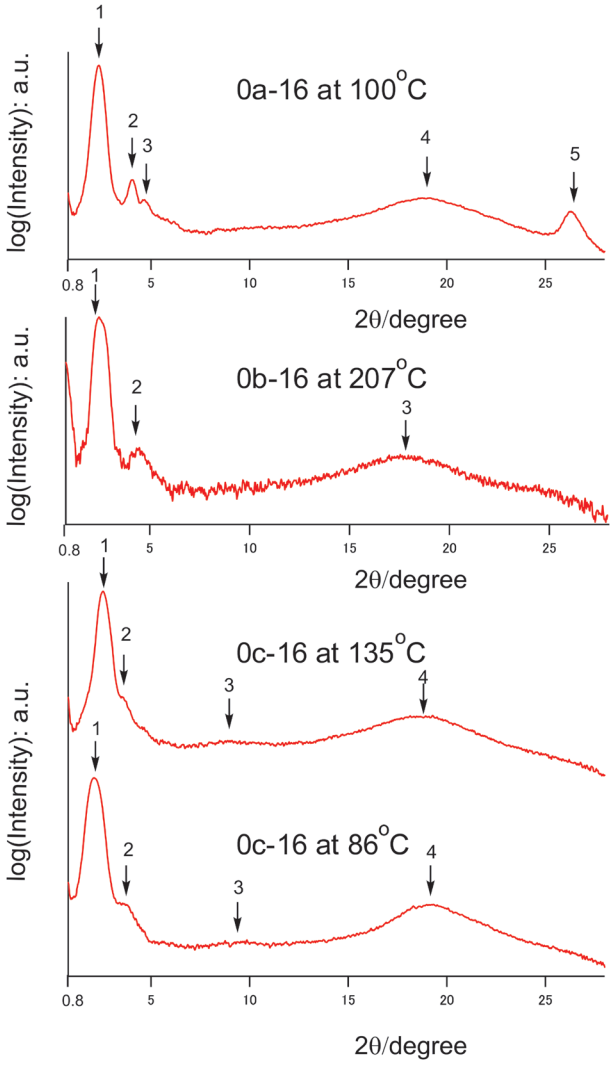

Fig. 8. X-ray diffraction patterns of the parent (4:0) compounds, **0a-16**, **0b-16** and **0c-16**

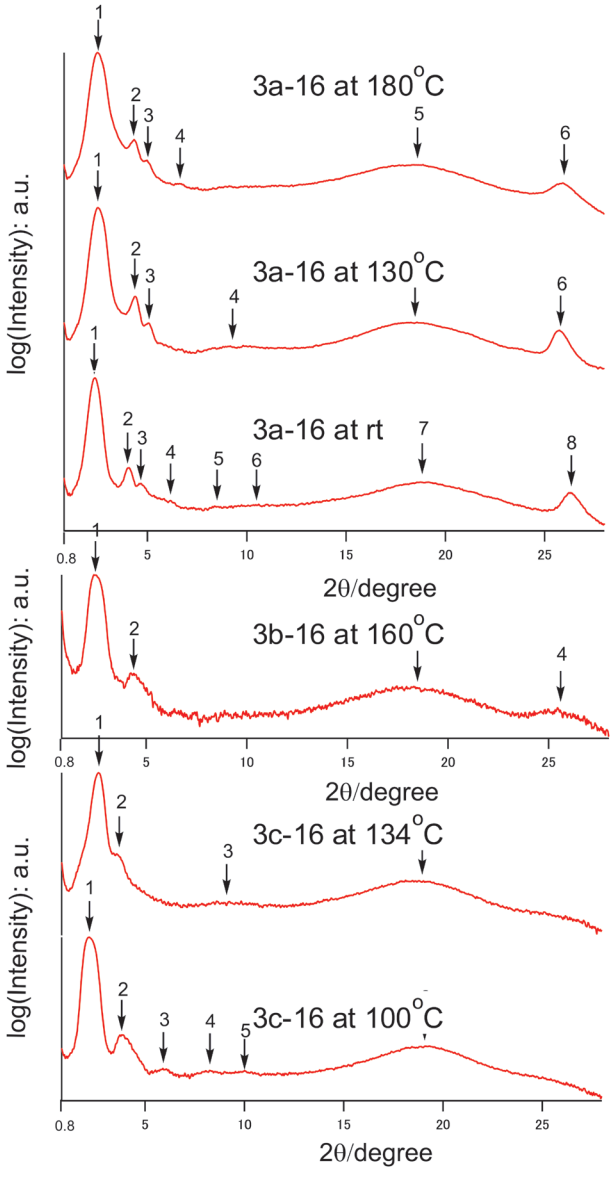

Fig. 9. X-ray diffraction patterns of the OH-substituted compounds, **3a-16**, **3b-16** and **3c-16**

region. In the highest angle region, a peak corresponding to the stacking distance in the columns could be also observed. As can be seen from the corresponding XRD data in Table 4, these mesophases could be identified as Col_{ho1} and Col_{ho2}. The mesophase of the *p-substituted* derivative **2b-16** could be also identified as Col_{ho}. However, as can be seen from Fig. 10, the (001) reflection (Peak No. 7) corresponding to the stacking distance in the highest angle region was considerably broader compared to the *m-substituted* derivative **2a-16**. When the density of this mesophase is assumed to be 0.90 $g \cdot cm^{-3}$, the number of molecules *Z* per unit lattice is just 1.0. This *Z* value is consistent with a Col_{ho} phase [31].

Figure 10 also shows the X-ray diffraction pattern of the mesophase at 120 °C in the *m,p-substituted* derivative **2c-16**. As can be seen from this X-ray pattern, the reflection peaks of the *m,p-substituted* derivative **2c-16** were broad and smaller in number than the *m-substituted* derivative **2a-16** and the *p-substituted* derivative **2b-16**. However, as can be seen from Table 4, there was no contradiction for the assignment to the Col_{hd} phase.

Furthermore, it is apparent from Fig. 10 that each of the OFBA-substituted compounds {**2a~2c-16**} gave no Peak H due to the helical supramolecular structure around 2θ = 1.0, similarly to the parent (4:0) compounds {**0a~0c-16**} and the OH-substituted compounds {**3a~3c-16**}.

***C_{60}-substituted compounds* {1a~1c-16}.** As can be seen from Fig. 11, the X-ray patterns of the *m-substituted* $(PhO)_6PcCu\text{-}C_{60}$ dyad **1a-16** and the *p-substituted* $(PhO)_6PcCu\text{-}C_{60}$ dyad **1b-16** were broader and fewer in number, in comparison with the precursors of the *m-substituted* derivative **2a-16** and *p-substituted* derivative **2b-16** (in Fig. 10). However, similarly to the precursors **2a-16** and **2b-16**, the $(PhO)_6PcCu\text{-}C_{60}$ dyads **1a-16** and **1b-16** gave a (001) reflection in the highest

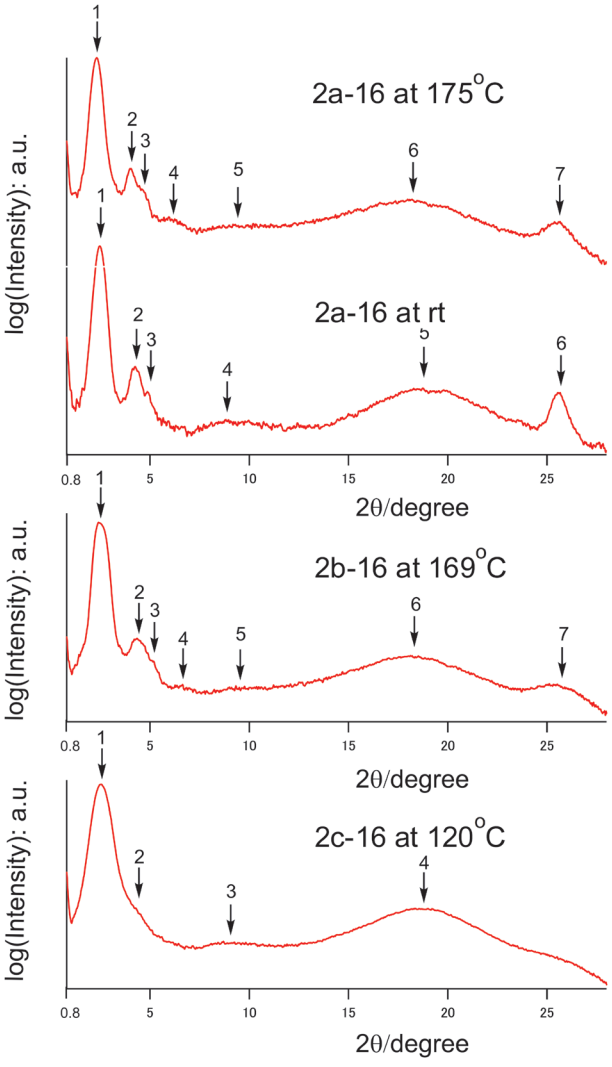

Fig. 10. X-ray diffraction patterns of the OFBA-substituted compounds, **2a-16**, **2b-16** and **2c-16**

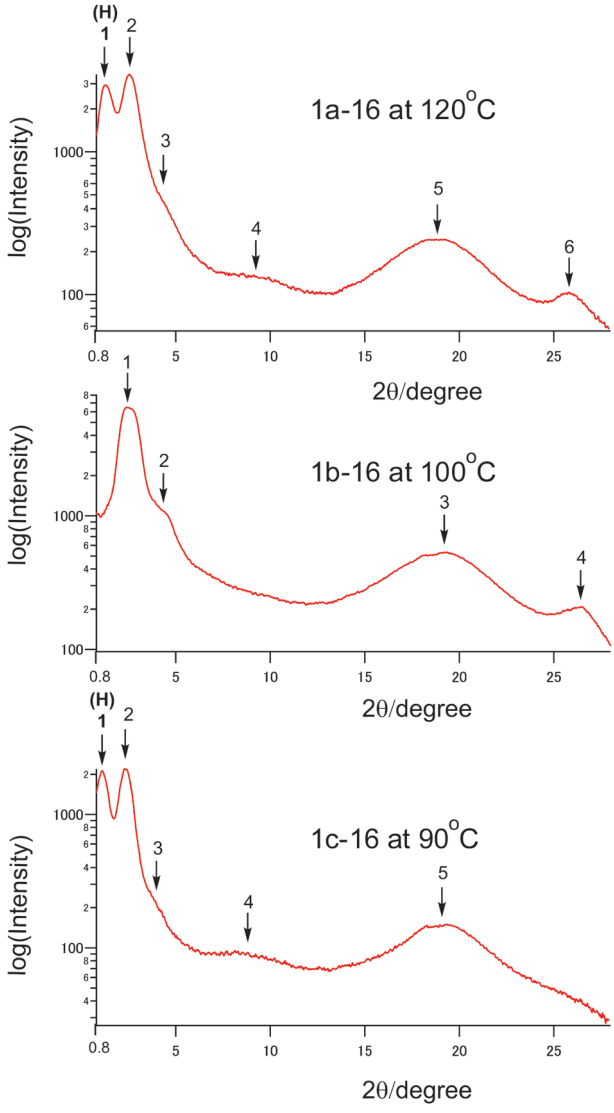

Fig. 11. X-ray diffraction patterns of the **$(PhO)_6$PcCu-C_{60}** derivatives: **1a-16**, **1b-16** and **1c-16**

angle region due to the stacking distance (h). On the other hand, the *m,p*-substituted **1c-16** gave no (001) reflection in the highest angle region due to the stacking distance (h). As can be seen from Table 4, the mesophases of the *m-substituted* derivative **1a-16,** the *p-substituted* derivative **1b-16** and the *m,p-substituted* derivative **1c-16** could be assigned without contradiction as the Col_{ho}, Col_{ho} and Col_{hd} phases, respectively.

Furthermore, as can be seen from Fig. 11, the *m-substituted* derivative **1a-16** and the *m,p-substituted* derivative **1c-16** showed a very big Peak H (Peak No. 1) around $2\theta = 1.1$ due to the helical supramolecular structure, whereas no Peak H appeared in the *p-substituted* derivative **1b-16**. It is very interesting that Peak H did not appear only in the *p-substituent* derivative **1b-16**. Therefore, it is also interesting for us that another research group reported the helical peak appeared in the *p-substituted* $(PhO)_6$PcCu-C_{60} dyad [= ZnPc-C_{60}] [10, 15, 16, 26].

This *p-substituted* ZnPc-C_{60} dyad showed a Peak H as only a very small shoulder (see Fig. 2(d) in Ref. 16), whereas our *m,p-substituted* dyads showed it as an extremely big clear peak [21, 22, 24, 25]. Moreover, this PcZn-C_{60} dyad shows only rectangular columnar (Col_r) phases, so that the dyad cannot achieve homeotropic alignment. In principle, only hexagonal columnar (Col_h) and tetragonal columnar (Col_{tet}) phases can give a homeotropically aligned sample [28]. Therefore, it might be impossible for these Col_r phases to prepare the homeotropically aligned samples for the proof of the helicity by the X-ray diffraction technique Method C [21]. However, the caption of Fig. S5 of their supplementary information, says, "XRD patterns of ZnPc-C_{60} [= (p-C_{12}OPhO)$_6$PcZn-OPh-C_{60}] films oriented in the direction of (a) parallel to X-ray beam (solid line) and (b) perpendicular to the X-ray beam (dashed line) [16]". From this expression, it is unknown where the Z-axis directions in the columns are actually in the samples (a) and (b): it is also unknown whether these films (a)

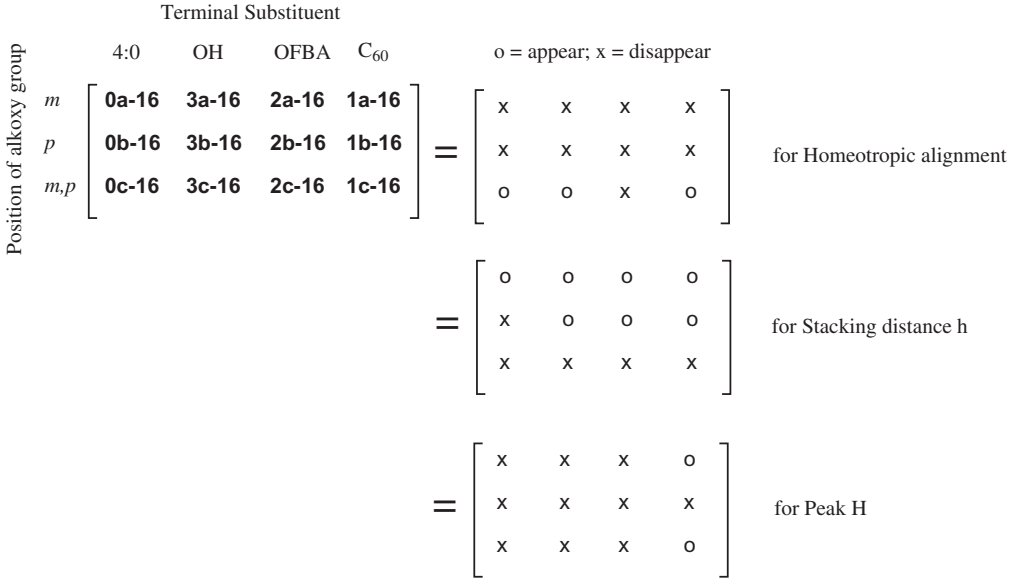

Fig. 12. Influence of the terminal substituent and the position of the alkoxy group on the appearance of homeotropic alignment, staking distance h and Peak H

0a-16: (m-C_{16}OPhO)$_8$PcCu; 3a-16: (m-C_{16}OPhO)$_6$PcCu-OH; 2a-16: (m-C_{16}OPhO)$_6$PcCu-OFBA; 1a-16: (m-C_{16}OPhO)$_6$PcCu-C_{60};
0b-16: (p-C_{16}OPhO)$_8$PcCu; 3b-16: (p-C_{16}OPhO)$_6$PcCu-OH; 2b-16: (p-C_{16}OPhO)$_6$PcCu-OFBA; 1b-16: (p-C_{16}OPhO)$_6$PcCu-C_{60};
0c-16: [m,p-(C_{16}O)$_2$PhO]$_8$PcCu; 3c-16: [m,p-(C_{16}O)$_2$PhO]$_6$PcCu-OH; 2c-16: [m,p-(C_{16}O)$_2$PhO]$_6$PcCu-OFBA; 1c-16: [m,p-(C_{16}O)$_2$PhO]$_6$PcCu-C_{60}

and (b) are homogeneous and homeotropic, respectively. Since there is no description about how to prepare these samples (a) and (b), the other researchers cannot carry out the replications. If the sample (a) is homogeneously aligned, the 1D helical peak in the Z-axis direction should appear but the reflection peaks from the 2D lattice of the columns in the XY-direction should disappear (see Method B in Ref. 21). Accordingly, the 2D peak of (200) should disappear. However, it appears as a large peak in the XRD in Fig. S5 (a). This is contradictory to the principle. Also, if the sample (b) is homogeneously aligned, the 1D peak due to the helix in the Z-axis direction should disappear but the reflection peaks due to the 2D packing of columns in the XY-direction should appear (see Method C in Ref. 21). Since the peak assigned to the helicity in the Z-axis direction disappeared in Fig. S5 (b), the sample (b) should be a homeotropically aligned sample. However, the evidence of the homeotropic alignment by using a polarizing microscope was not written. Therefore, this proof has not satisfactorily carried out for the helicity of the ZnPc-C_{60} dyad [10, 15, 16, 26]. Even for the *p*-substituent dyad ZnPc-C_{60}, they should first prove the homeotropic alignment by the method using the polarization microscope, and then the XRD should be taken for the surely homeotropically-aligned sample. Moreover, the XRD pattern of a Col_r phase generally gives two strong reflections from the (110) and (200) planes, because these two planes are the densest in the molecular net planes. However, the (110) reflection is absent in this indexation for these Col_r phases [16]. From these scientific viewpoints, this phase identification is not satisfactory. Therefore, it may be required to reinvestigate the X-ray structural analysis for the helicity and the mesophase assignment for the ZnPc-C_{60} dyad based on *p-substituent* (PhO)$_6$PcM-C_{60} system.

Effect of position of alkoxy group and kind of terminal substituent on appearance of homeotropic alignment, stacking h and Peak H

As described above, it was found that the substitution position of the alkoxy group and the type of terminal substituent greatly influence the appearance of homeotropic alignment, stacking h and Peak H. Therefore, the relationship is summarized in matrix form in Fig. 12.

As can be seen from these matrixes, the homeotropic alignment tends to appear only in the *m,p-substituted* derivatives, regardless of the terminal substituent. The stacking distance h tends to appear in the *m-substituted* and *p-substituted* derivatives, but not in the *m,p-substituted* derivatives, regardless of the terminal substituent. On the other hand, Peak H tends to appear only in the *C_{60}-substituted* derivatives but not in all the other derivatives, regardless of the substitution position of the alkoxy group.

Hereupon, it can be seen from these matrixes that only the *m,p-substituted* derivative **1c-16** is a sample suitable

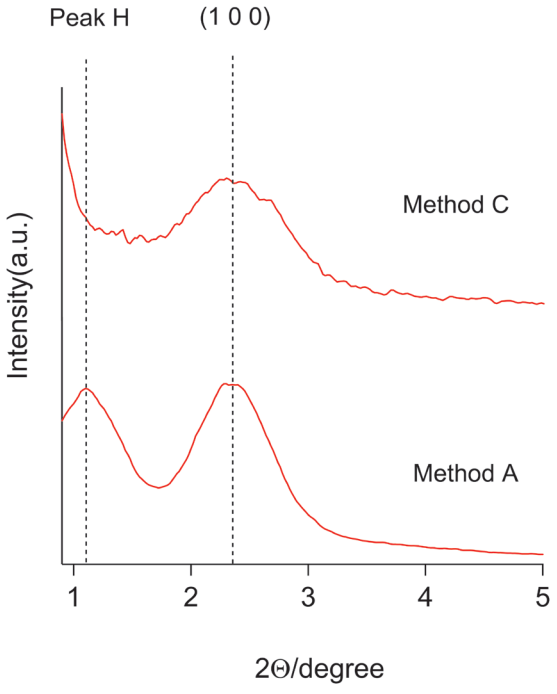

Fig. 13. Small angle X-ray diffraction patterns of the non-aligned sample **[*m,p*-$(C_{16}O)_2$PhO]$_6$PcCu-C_{60}** (**1c-16**) at 90 °C. for Method A and the homeotropically aligned sample between two glass plates for Method C

for the measurement using Method C in Fig. 7, because it must be a sample showing Peak H with homeotropic alignment.

Fig. 13 shows the X-ray patterns of the Col_{hd} mesophase in the *m,p-substituted* derivative **1c-16** measured with Method A and Method C. As can be seen from this figure, when the non-aligned sample was measured with Method A, both Peak H and (100) reflection peak could be observed. On the other hand, when the homeotropically aligned sample was measured with Method C, the (100) reflection could be observed but the Peak H disappeared. This means that Peak H is a periodicity along the Z-axis direction of the column as illustrated in Fig. 7. Therefore, it could be concluded that Peak H corresponds to the pitch of C_{60} stacked spirally around the column in the Z-axis direction. This is also supported from previous studies [21, 22, 24, 25]. In our previous work, a very precise argument was already described for the homologous derivative **1c-10**: [*m,p*-$(C_{10}O)_2$PhO]$_6$PcCu-C_{60}. The number of the C_{60} molecules per the pitch could be estimated to be about 16 and 23.4° for the rotation angle of the dyads [21].

Thus, it was proven from the measurements with both Methods A and C that Peak H in the *m,p-substituted* derivative **1c-16** originates from a helical pitch of C_{60}.

As can be seen from the above description, a sample showing Peak H with homeotropic alignment must be needed for the helicity proof by using XRD Method C in Fig. 7. The helical peak in the *p-substituted* $(PhO)_6$PcCu-C_{60} dyad [= ZnPc-C_{60}] reported by another research group [10, 15, 16, 26] should be proven by Method C for the sample showing both Peak H and homeotropic alignment.

Reason why Peak H (C_{60} helix) appears

Figure 14 schematically illustrates a possible reason why the helicity of C_{60} moieties appears in the *m-substituted* derivative **1a-16** and the *m,p-substituted* derivative **1c-16** but not in the *p*-substituent derivative **1b-16**.

In this figure, the green circle represents the phthalocyanine (Pc) ring, and both the light blue and pale yellow circles represent the long chain alkoxy chains at the *m*- and *p*-positions, respectively. In the *m-substituted* derivative **1a-16**, the long alkoxy chains may extend downward from the plane of the Pc ring, because they are substituted at the *m-position* of the phenoxy groups whose planes are almost perpendicular to the Pc ring plane by their steric hindrance. Therefore, the light blue circle of the long alkoxy chains may be small as illustrated in this figure. On the other hand, in the *p-substituted* derivative **1b-16**, the long alkoxy chains may extend in the same plane as the Pc ring, because they are substituted at the *p*-position of the phenoxy groups. Therefore, the pale yellow circle of the long alkoxy chains in *p-substituted* derivative **1b-16** may be much larger than the blue circle of the *m-substituted* derivative **1a-16**, as illustrated in this figure. In the *m,p-substituted* derivative **1c-16**, the long alkoxy chains at the *m*-position and the *p*-position may extend as in the *m-substituted* derivative **1a-16** and in *p-substituted* derivative **1b-16**, respectively.

In the *m-substituted* derivative **1a-16**, the hydrophilic fullerenes (C_{60}s) may be excluded outside the skirt formed by the hydrophobic long alkoxy chains, so that the fullerenes can easily aggregate in a helical form. In the *p-substituted* derivative **1b-16**, the aggregation of the fullerenes may be thermally disturbed by the molten long alkoxy chains in the same plane to prevent formation of helical stacking of fullerenes. On the other hand, in the *m,p-substituted* derivative **1c-16**, the fullerenes can be excluded outside the skirt formed by the long alkoxy chains at the *meta* position, even though the long alkoxy chains are substituted also at the *p*-position. Thus, a helical aggregation of fullerenes may also form in the *m,p-substituted* derivative **1c-16**. It is apparent from our results mentioned above that the *m-substituted* long alkoxy chains are needed to form the helical supramolecular structure of fullerenes in this type of dyad based on $(PhO)_6$PcM-C_{60}. For more general compounds, further studies are necessary to prove this hypothesis.

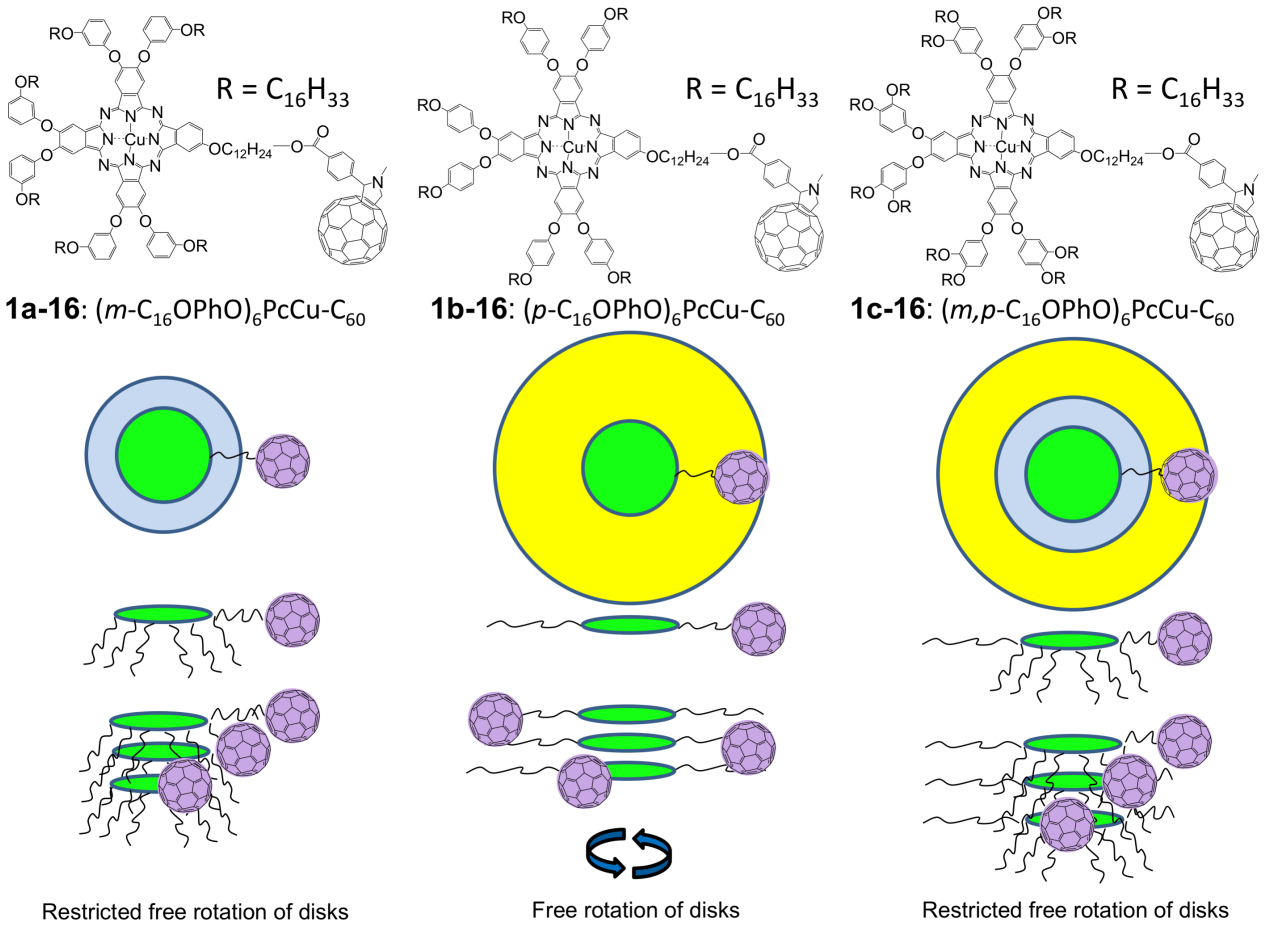

Fig. 14. Possible reason why the helicity of C_{60} moieties appears for **1a-16** and **1c-16** but not for **1b-16**

CONCLUSION

In this study, we have synthesized twelve novel discotic liquid crystals based on a phthalocyaninato copper(II) complex having the same alkoxy chain of $C_{16}H_{33}O$: the parent (4:0) compounds (**0a-16, 0b-16**, **0c-16**), the OH-substituted compounds (**3a-16, 3b-16**, **03c-16**), the OFBA-substituted compounds (**2a-16, 2b-16**, **2c-16**) and the C_{60}-substituted dyads (**1a-16, 1b-16**, **1c-16**). The letters of **a**, **b** and **c** with the entry numbers mean the *m-substituted* derivative, *p-substituted* derivative and *m,p-substituted* derivative, respectively. The abbreviations of OH, OFBA and C_{60} indicate the terminal groups of the bridge in the children (3:1) compound. We have investigated the influence of both substitution position of the alkoxy chains and the type of terminal group on the mesomorphism, the homeotropic alignment, the stacking distance h and the helical supramolecular structure, by using DSC, POM and temperature-variable small angle X-ray diffraction measurements. As a result, each of the derivatives shows columnar mesophase(s). The homeotropic alignment tended to appear only in the *m,p-substituted* derivatives, regardless of the terminal substituents (OH, OFBA and C_{60}). In addition, the stacking distance h tends to appear in the *m-substituted* and *p-substituted* derivatives, but not in the *m,p-substituted* derivatives, regardless of the terminal substituents (OH, OFBA and C_{60}). On the other hand, an additional big peak (Peak H) tends to appear at around $2\theta = 1.1°$ in the X-ray diffraction patterns for the *C_{60}-substituted* dyads {**1a~1c-16**} but not for the other compounds, {**0a~0c-16**}, {**3a~3c-16**} and {**2a~2c-16**}, regardless of the substitution positions (*m-*, *p-* and *m,p-*) of the alkoxy group. Moreover, we revealed that both the *m-substituted* derivative **1a-16** and the *m,p-substituted* derivative **1c-16** gave Peak H, but that only the *p-substituted* derivative **1b-16** did not give Peak H among these three dyads {**1a~1c-16**}. From the temperature-variable small angle X-ray diffraction measurements for the *m,p-substituted* derivative **1c-16** using two different sample preparation methods, we proved that the Peak H is originated from a helical pitch of fullerenes. We also pointed out that the *m-substituted* long alkoxy chains at least are needed to form the helical supramolecular structure in the present $(PhO)_6PcM\text{-}C_{60}$-based dyads.

REFERENCES

1. Part 55: Yatabe M, Kajitani A, Yasutake M and Ohta K. *J. Porphyrins Phthalocyanines* 2018; **22**: 32–45.
2. Bushby JR, Hamley IW, Liu Q, Lozman OR and Lydon EJ. *J. Mater. Chem.* 2005; **15**: 4429–4434.
3. Uchida S, Kude Y, Nishikitani Y and Ota (= Ohta) K. *Jpn. Kokai Tokkyo Koho* JP 2008214227(A)-2008-09-18 (Priority number: JP2007060604; Submission Date: 2007-03-09).
4. de la Escosura A, Martınrez-Dıaz MV, Barbera J and Torres T. *J. Org. Chem.* 2008; **73**: 1475-1480.
5. Tauchi L, Shimizu M and Ohta K. The Proceedings of Annual Conference of Japanese Liquid Crystal Society, 2009-09-13~15; C02.
6. Ota (= Ohta) K. *Jpn. Kokai Tokkyo Koho* 2011; JP2011132180(A)-2011-07-07 (Priority number: JP20090293501; Submission Date: 2009-12-24).
7. Geerts YH, Debever O, Amato C and Sergeyev S. *Beilstein J. Org. Chem.* 2009; **5**: 1–9.
8. Nguyen-Tran HT, Tauchi L, Kamei T and Ohta K. *The Proceedings of the 90th CSJ Annual Meeting*, 2010-03-26~29; 3 E4:06.
9. Tauchi L, Shimizu M, Fujii T, Nguyen-Tran H-D, Kamei T and Ohta K. *The Proceedings of the 23rd International Liquid Crystal Conference*, Krakow, Poland, 2010-07-11~16; P1.106.
10. Nihashi W, Hayashi H, Shimizu Y, Umeyama T and Matano Y and Imahori H. *The Proceedings of the 39th Symposium on the Fullerens, Nanotubes and Graphene Research Society*, 2010-09-07; 3P–2.
11. Ohta K, Tauchi L, Nguyen-Tran HT, Shimizu M, Kamei T and Kato T. *The Proceedings of Pacifichem 2010*, Hawaii, USA, 2010-12-15~19; MATL-255 (Invited Lecture).
12. Tauchi L, Shimizu M, Ohta K and Itoh E. *The Proceedings of Pacifichem 2010*, Hawaii, USA, 2010-12-15~19; MATL-795.
13. Nguyen-Tran H-T, Tauchi L, Kamei T, Kato T, Ohta K and Itoh E. *The Proceedings of Pacifichem 2010*, Hawaii, USA, 2010-12-15~19; MATL-797.
14. Nakagaki T, Tauchi L, Shimizu M and Ohta K. *The Proceedings of the 91st CSJ Annual Meeting*, 2011-03-26~29; 3D3-55.
15. Nihashi W, Hayashi H, Umeyama T, Matano Y and Imahori H. *The Proceedings of the 91st CSJ Annual Meeting*, 2011-03-26~29; 2F2-13.
16. Hayashi H, Nihashi W, Umeyama T, Matano Y, Seki, S, Shimizu Y and Imahori H. *J. Am. Chem. Soc.* 2011; **133**: 10736–10739 (submission date: 2011-04-26) published 2011-06-23).
17. Bagui M, Dutta T, Chakraborty S, Melinger JS, Zhong H, Keightley A and Peng Z. *J. Phys. Chem. A* 2011; **115**: 1579–1592.
18. Ince M, Martinez-Diaz MV, Barbera J and Torres T. *J. Mater. Chem.* 2011; **21**: 153: 1–1536.
19. Kamei T, Kato T, Itoh E and Ohta K. *J. Porphyrins Phthalocyanines* 2012; **16**: 1261–1275.
20. Shimizu M, Tauchi L, Nakagaki T, Ishikawa A, Itoh E and Ohta K. *J. Porphyrins Phthalocyanines* 2013: **17**: 264-282.
21. Tauchi L, Nakagaki T, Shimizu M, Itoh E, Yasutake M and Ohta K. *J. Porphyrins Phthalocyanines* 2013: **17**: 1080–1093.
22. Ishikawa A, Ono K, Ohta K, Yasutake M, Ichikawa M and Itoh E. *J. Porphyrins Phthalocyanines*, 2014; **18**: 366–379.
23. Yoshioka M, Ohta K, Miwa M, Kutsumizu S and Yasutake M. *J. Porphyrins Phthalocyanines*, 2014; **18**: 856–868.
24. Watarai A. Yajima S. Ishikawa A. Ono K. Yasutake M and Ohta K. *ECS Transactions*, 2015; **66**: 21-43.
25. Watarai A, Ohta K, Yasutake M. *J. Porphyrins Phthalocyanines*, 2016; **20**: 1444–1456.
26. Hayashi H, Nihashi W, Umeyama T, MatanoY, Seki S, Shimizu Y and Imahori H. *J. Amer. Chem. Soc.* 2017; **139**: 13957–13957. Correction to Ref. 16.
27. Yoshikawa S. Chemistry & Chemical Industry, 2006; **59**: 960-963.
28. Hatsusaka K, Ohta K, Yamamoto I and Shirai H. *J. Mater. Chem.* 2001; **11**: 423–433.
29. Ichihara M, Suzuki A, Hatsusaka K and Ohta K. *J. Porphyrins Phthalocyanines* 2007; **11**: 503–512.
30. Sato H, Igarashi K, Yama Y, Ichihara M, Itoh E and Ohta K. *J. Porphyrins Phthalocyanines* 2012; **16**: 1148–1158.
31. (a) Ohta K. "Dimensionality and Hierarchy of Liquid Crystalline Phases: X-ray Structural Analysis of the Dimensional Assemblies," Shinshu University Institutional Repository, submitted on 11 May, 2013; http://hdl.handle.net/10091/17016; (b) Ohta K. "Identification of discotic mesophases by X-ray structure analysis," in "Introduction to Experiments in Liquid Crystal Science (Ekisho Kagaku Jikken Nyumon [in Japanese])," ed., Japanese Liquid Crystal Society, Ch. 2-(3), pp. 11–21, Sigma Shuppan, Tokyo, 2007; ISBN-13: 978-4915666490.